Spring 2017

Magneto inductive communication system for underwater wireless sensor networks

Niaz Ahmed

Department: Electrical and Computer Engineering

MAGNETO INDUCTIVE COMMUNICATION SYSTEM FOR UNDERWATER WIRELESS SENSOR NETWORKS

by

NIAZ AHMED

A DISSERTATION

Presented to the Graduate Faculty of the

MISSOURI UNIVERSITY OF SCIENCE AND TECHNOLOGY

In Partial Fulfillment of the Requirements for the Degree

DOCTOR OF PHILOSOPHY

in

ELECTRICAL ENGINEERING

2017

Approved by

Yahong Rosa Zheng, Advisor
David Pommerenke
Sahra Sedigh Sarvestani
Amardeep Kaur
Haoyi Xiong

PUBLICATION DISSERTATION OPTION

This dissertation has been prepared using the Publication Option. The dissertation consists of the following published or to be published papers, formatted in the style used by the Missouri University of Science and Technology, listed as follows:

Paper I, (pages 6–32) N. Ahmed, A. Radchencko, D. Pommerenke and Y. R. Zheng, "Low-Cost Wireless Sensors Using Magnetic Induction for Underwater and Underground Communications," submitted to IEEE Sensors Journal, March 2017.

Paper II, (pages 33–47) N. Ahmed, Y. R. Zheng and D. Pommerenke, "Theoretical Modeling of Multi-Coil Channels in near Field Magneto-Inductive Communication," IEEE 82nd Vehicular Technology Conference (VTC2015-Fall), Boston, MA, September 2015.

Paper III, (pages 48–58) N. Ahmed, Y. R. Zheng and D. Pommerenke, "Effects of Metal Structures On Magneto-Inductive Coupled Coils," IEEE Third Underwater Communications and Networking Conference (UComms16), Lerici, Italy, August 2016.

Paper IV, (pages 59–72) N. Ahmed, Y. R. Zheng and D. Pommerenke, "Multi-coil MI based MAC protocol for wireless sensor networks," MTS/IEEE OCEANS'16 conference , Monterey, CA, September 2016.

ABSTRACT

Underwater wireless sensor networks have found a number of applications in underwater environment monitoring, infrastructure monitoring, military applications and ocean exploration. Among the four possible means of underwater wireless communication, namely acoustic, electromagnetic (EM), magneto-inductive (MI) and optics communication, MI communication enjoys the advantages of being low cost and robust equally in air, water and soil. This dissertation presents design and implementation of a low-power and low-cost MI sensor network node that is suited for long-term deployment of underwater and underground infrastructure monitoring, such as bridge scour and levee scour monitoring. The designed MI sensor node combat the directionality of the single coil MI communication by utilizing 3D coil to both transmit and receive. The presented MI sensor node is tested in air and underwater to show robustness and reliability. The sensor node is designed after thorough analysis and evaluation of various MI challenges such as directionality, short range, decoupling due to mis-alignment of coils, and effect of metal structure. A communication range of 40 m has been achieved by the prototype sensor node. The prototyping cost of a sensor node is less than US$100 and will be drastically reduced at volume production. A novel and an energy efficient medium access control (MAC) protocol based on the carrier sense medium access (CSMA) has also been implemented for the designed sensor node to improve throughput in a dense network.

ACKNOWLEDGMENTS

First and foremost, I would like to acknowledge my advisor Dr. Yahong Rosa Zheng. I sincerely appreciate her continuous support and devoted guidance throughout my Ph.D study. Without her numerous constructive suggestions, insightful comments and generous financial support, this dissertation would have been impossible. She has also provided me the opportunity to lead undergraduate students, indulge in entrepreneur programs which helped me to improve my leadership and entrepreneur ship skills. Her enthusiasm, dedication and down-to-earth attitude towards research have set a role model of academic perfection, from which I will benefit in my future research career.

My deep appreciation also goes to Dr. David Pommerenke for his guidance and continuous help with hands on skills in hardware design, implementation and field experiments. He also used to share his experience to teach me working efficiently and diligently.

I would like to thank the members of my advisory committee, Drs. Sahra Sedigh, Amardeep Kaur, and Haoyi Xiong, for generously offering their time and invaluable advice for my research.

I thank all the current members, Xiahan Yang, Huai Huang, Hussam Nassr, Yiheng Wang, Juening Jin, Aysen Malone and past members, Weimin Duan, Dongjie Bi, Ming Yue, Zengli Yang, Justin Hoytt and Caleb Olson for their kind support and friendship. I cherish the time we spent together in Rolla.

I would like to express my eternal gratitude to my family and parents for their unselfish love, everlasting support, prayers and sacrifice throughout these years.

TABLE OF CONTENTS

Page

LIST OF ILLUSTRATIONS

LIST OF TABLES

SECTION

1. INTRODUCTION

Underwater wireless sensor networks have been the area of during the last two decades due to a huge number of applications in environmental monitoring, military applications and ocean exploration. Advancement in underwater communication has been slow because of the research challenges offered due to lack of reliable mode of communication. The concepts of wireless communication mediums used in terrestrial communication such as electromagnetic waves (EM) and optical waves can not be simply applied to underwater because of the harsh environment. EM waves undergo high attenuation in water due to higher electric permittivity of water and are suitable for shallow and extremely short range communications only. Similarly, optical waves scatter in water and can be used for extremely short range applications. The commonly used medium for underwater communication is acoustics but the slow speed of propagation, severe multi-path and high cost of acoustic modems makes the acoustic communication very challenging. Recently, the use of Magneto Inductive (MI) communication has been studied for air, underground and underwater communications and found to be a promising choice to be used for underwater sensor networks applications.

MI communication is achieved using tightly tuned coils with quasi static field. The magnetic field is produced when a time-varying current passes through a conducting wire or a coil. The magnetic field lines when pass through the second coil, a voltage is induced. The transmit and receive coils resonate at frequency related to the load impedance. This resonance occurs when the transmit coil has minimum RLC series impedance and the receiver coil has maximum RLC parallel impedance as shown in Figure 1.1. The amount

of induced voltage is proportional to the fraction of magnetic flux lines generated by the first coil. Factors such as the current, size, shape of the coil and the separation distance between the two coils greatly effect the voltage induced in the second coil.

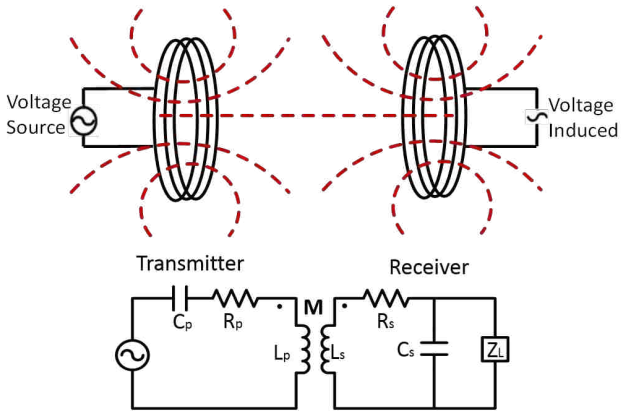

Figure 1.1. MI coupling

MI depends on relative permeability and conductivity of the medium. Magnetic permeability of rock, soil, and water is very similar (≈ 1), that makes MI very robust in all these mediums. The conductivity of the medium affects MI communication because of the eddy current produced due to the time varying field. This is measured by the skin depth and is given as

$$\delta = \sqrt{\frac{2}{\omega \mu_0 \sigma}}$$

where ω is the frequency and σ is the conductivity of the media and μ_0 is the magnetic permeability of free space. Thus, environments such as ocean where the water is salty and more conductive the skin effect will be more dominant and affect the communication. It can be seen that skin effect is directly proportional to the frequency and lowering the frequency can help to reduce the skin effect. On the other hand, using low frequencies magnetic channel suffers from a lot of background noise which also disrupt the communication. To cope with such background noise, transceivers are configured to work with extremely narrow bands.

MI communication offers a lot of underwater and underground structural monitoring applications especially bridge scour monitoring and levee scour monitoring. Bridge scouring and levee scouring is a process where running water erodes the sand and rocks from around the structure pillars causing to collapse. The structure collapse could occur in days, months or years. To control the damage the health of the structure needs to be monitored. Several methods have been proposed to monitor the structure health, such as magnetic sliding collars, sonar systems, remotely controlled boats, buried probes, fathometers and optical sensors but due to extreme rough conditions in a river flow these solutions does not appear a low cost and real time solution. There is a need of deploying on ground solution which can consistently monitor the structure. The dissertation presents design and implementation of MI sensor node that can be a real time solution for structural health monitoring applications.

Figure 1.2a shows the proposed solution for bridge scour monitoring where the sensor node is deployed with the bridge pillar. The sensor node is equipped with accelerometer which monitors the movement and position of the sensor node all the time. As the bridge scouring occurs, the sensor node will slide or experience a change in its position and will send that information back which will raise the scouring alert. Similarly, Figure 1.2b shows the proposed solution for levee scour monitoring where the sensor node is deployed with the I-wall. The sensor node is equipped with inclinometer which measures the tilt of the I-wall all the time. As the erosion occurs the I-wall tilts and the inclinometer will record the degree of inclination and report back to the base station.

1.1. PROBLEM STATEMENT

Wireless sensor networks in general are energy hungry networks. The sensor nodes are mostly battery powered and deployed in remote places where replacing power supply of the sensor node is hard. Energy efficiency is thus an important challenge for wireless sensor networks and especially for underwater structural monitoring applications where

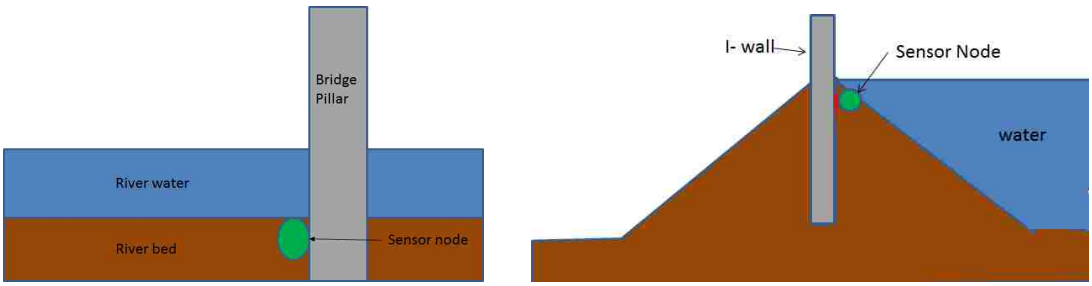

(a) Bridge scour monitoring (b) Levee scour monitoring

Figure 1.2. Bridge and Levee scouring solution

long term deployment is required. Along with the main challenge of designing a low power MI sensor node, MI also offers some challenges which are analyzed and taken care of in this dissertation.

Magnetic fields are directional and require the transmit and receive nodes to maintain a specific orientation. Keeping a sensor node with fixed orientation is not possible when deployed in field. This directional property of MI greatly affects the robustness and increases localization challenges too. This require the MI sensor node to be omni-directional which can be achieved by using three dimensional coils. Designing the three dimensional coil also needs a careful study as the mutual coupling between the coils can affect the performance. Using the three dimensional coils also has a trade-off between the communication distance and power consumption and require an optimal configuration.

The structural monitoring applications require the sensor nodes to gather the data through the sensors and report to a central position. During normal hours of operation, transmission activity is very low but can experience high traffic in case of emergency. This requires the sensor node to have an efficient MAC protocol that can guarantee successful transmission in case of failure detection.

1.2. CONTRIBUTIONS

The dissertation targets all the challenges and presents a low-power and low-cost practical solution to underwater wireless sensor networks using MI communication. The specific contributions are:

1. Hardware and software implementation of a robust and omni-directional MI sensor node that can be used in underwater structural monitoring applications. Analysis of three possible configurations of the 3D coil for MI transceiver are performed to choose the optimal configuration. Experimental evaluation of the MI sensor node in air and underwater are also conducted to verify the robustness and performance (presented in Paper 1).

2. Theoretical model is derived for 3D coil MI transceiver to calculate the mutual coupling between the receive and transmit coils. Equivalent circuit analysis are also performed for the 3D coil to observe the effect of detuning and mis-alignment (presented in Paper 2).

3. Analysis of the effect of metal structures near MI nodes have been carried out using EMCoStudio simulations. Our analysis have shown that metal structures greatly affect the communication performance and found the minimum separation that MI node can have from the metal structure (presented in Paper 3).

4. Implementation of an energy efficient MAC protocol that utilizes the directional pattern of the magnetic field produced through each of the three coils. (presented in Paper 4).

PAPER

I. LOW-COST WIRELESS SENSORS USING MAGNETIC INDUCTION FOR UNDERWATER AND UNDERGROUND COMMUNICATIONS

Niaz Ahmed, Andriy Radchencko, David Pommerenke, Y. Rosa Zheng

Dept. of Electrical & Computer Engineering

Missouri University of Science & Technology, Rolla, MO 65409

{namn3, zhengyr}@mst.edu

ABSTRACT

A set of low-cost wireless sensors are designed and implemented using Magnetic Induction (MI) for underwater and underground communications. Hardware features of the sensor nodes include a 3D MI coil antenna and its different configurations for transmit and receive operations, low-power circuits for sleep mode, several types of sensors, data storage, and best transmit/receive circuits selected to achieve the maximum communication range with low power consumption. The material cost of a sensor node is less than US$100 at the prototyping stage and can be drastically reduced at volume production. Software designs utilize low-power modes of micro-controllers and power supply circuits, state-machine implementation of sleep, receive, sensing, and transmit modes, range estimation from RSSI (received signal strength indicator), and medium access protocols such as polling and CSMA (carrier sensing multiple access). Extensive lab and field tests conducted with the sensor nodes demonstrate promising performance in terms of power consumption, communication range, range estimation, and robustness against mismatch of coil orientations and networking capabilities.

1. INTRODUCTION

Wireless sensor networks have been widely applied to environmental monitoring, infrastructure monitoring, smart living, smart manufacturing, etc. In particular, underwater and underground sensor networks play a more important role in ocean exploration, coastal surveillance, infrastructure monitoring, and underground mining, as these environment is hostile to human operators, and robots and autonomous vehicles are expected to work with the wireless sensor networks in the access-denied environment. Example applications are non-destructive detection of water-front infrastructure defects [17], levee/river bank monitoring, pipe-line monitoring of undersea oil production and transportation, early warning of disastrous flood/storm, and ocean observatory, etc. For most of those applications, low-power consumption, long-deployment lifespan, sensing ability, and reliable communication are the key requirements to the sensor network nodes.

Unlike the common wireless sensors that use Radio Frequency (RF) propagation for communication in the air, underwater or underground wireless communications have proven to be extremely difficult [15, 11]. The possible means of wireless communication underwater/underground include optics [18, 6], acoustics [8, 21, 27, 26], and Magnetic Induction (MI) [23, 13, 3, 19, 10, 25, 2, 14, 22, 20, 11, 4, 16]. In the review papers [5, 9], the authors provide detailed comparison of the three communication means in ocean underwater environment. In comparison to acoustic and optical communications, MI communication has the advantage of be low cost, low power consumption, performs consistently in most communication media: in-air, underwater, and underground. Therefore, MI is suitable for wireless sensor networks deployed in all environment and with long-lifespan requirements.

Recent development in MI communication include nearfield touchless entry [13, 3, 16], RF identification (RFID) [25, 2], underground sensing [22], and target localization [19, 10]. A handful of existing MI communication systems are found in the literature for underwater and underground applications. In [20], a high magnetic moment (250 Am^2) at the transmitter was used to achieve 400 m communication range in sea water with a

low data rate (40 bps) and a low carrier frequency (< 3 kHz). In [11], the underwater MI channels are modeled by considering dense networks with closely placed transmitters and receivers. In [3], nearfield relaying of closely placed coils were investigated to increase the communication range. In [17, 4], we presented a low-cost MI sensor node that uses one transmit coil and one or three receive coils at 125 kHz carrier frequency to achieve 20 m range at 1 kbps data rate.

In this paper, we investigate three different transmission configurations through the 3D coils and their effects on communication range and power consumption. One transmit configuration is to connect the three coils in series and excite them simultaneously with one signal source (Figure 1a); the second configuration is to connect three coils with three separate signal sources and simultaneously transmit the three signals (Figure 1b); the third configuration is to connect the three coils with one signal source via a switch and transmit three separate signals sequentially in time (Figure 1c). Our study shows that the sequential transmission scheme has more advantage over the simultaneous transmission schemes in terms of omni-directionality and power consumption.

With the third configuration, we also provide an integrated solution to a low-power MI sensor node that achieves robust communication over 40 meter range and 1 kbps to 5 kbps data rate. With commercial of the shelf (COTS) components, the integrated sensor node has a small form factor, and a low material cost of less than US100. Sensing and data storage capability, range estimation, and medium access protocols are also implemented in the sensors. Laboratory and field tests demonstrate that the sensor nodes achieve good communication range and with very low power consumption.

2. PRINCIPLE OF MI COMMUNICATIONS

MI communications uses well-tuned coils to create an alternating magnetic field. If $\lambda/2\pi >> d$, where λ is the wavelength and d is the distance between the transmitter and receiver, then the magnetic field within the radius R is regarded as a quasi-static field or

near field. A single MI coil exhibits strong directionality, meaning that the magnetic field along its axis is stronger than that along the other directions. The induced voltage in the receive coil is higher when the receive coil faces the transmit coil than those when two cols are at different orientations. For this reason, multi-coil system is often necessary for MI communication systems to achieve near omni-directional communication in the three dimensional (3D) space. Similar to inductive power charging systems [7], three coils are often used together with their center coinciding at one point and their axes orthogonal to each other. This physical configuration helps achieving maximal strength in both transmission and reception, as well as the best omni-directionality [24, 12, 14]. However, different configurations of the three transmit and receive coils are available, and these configurations have rather different performance.

Three configurations are commonly used in the literature, as shown in Fig. 1. Configuration 1 uses a single signal source to excite the three coils connected in series. Configuration 2 uses three independent signal sources to excite each coil separately and simultaneously. The use of independent sources allows Configuration 2 to transmit either the same or different signals at a given time. Configuration 3 uses a single source to transmit sequentially through the three coils and the magnetic fields generated at different times may be combined differently, as shown in Fig. 1d.

The three dimensional coils are placed in a Cartesian coordinate system and $\hat{x}$, $\hat{y}$, and $\hat{z}$ are unit vectors that aligns with the three axes. Coil 1 is on the xy plane and its coil axis is $\hat{z}$, Coil 2 is on the xz plane with coil axis at $\hat{y}$, and Coil 3 is on the yz plane with coil axis at $\hat{x}$. With the coils centered at the origin, the magnetic field at an arbitrary observing point $s = (x, y, z)$ produced by the transmit coil i is derived by [19].

$$\mathbf{B}_i = C_0 I_i(t)(B_{ix}\hat{x} + B_{iy}\hat{y} + B_{iz}\hat{z}) \quad i = 1, 2, 3 \tag{1}$$

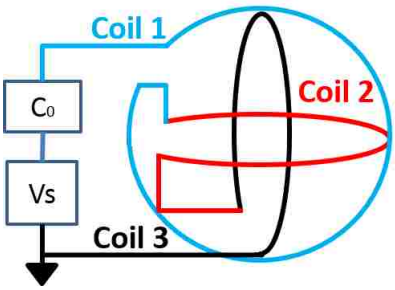

(a) Single source with coils connected in series

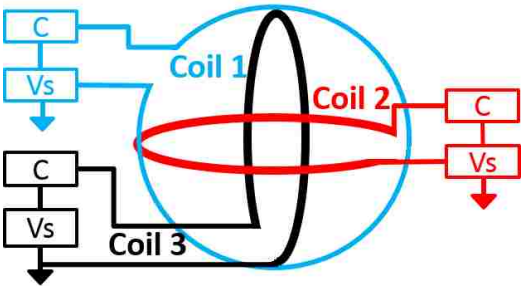

(b) Sperate sources connected with coils in parallel

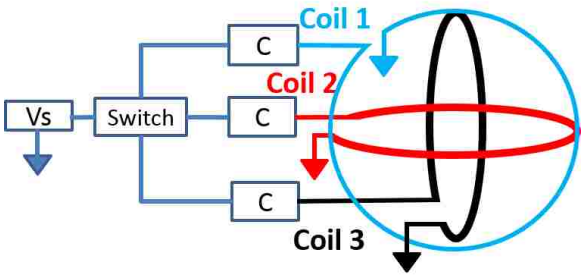

(c) Single source connected with coils in parallel and transmit in series

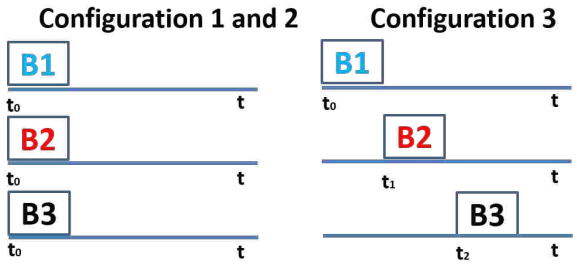

(d) Timing of magnetic fields in the three configurations.

Figure 1. Three configurations of the transmit coils. Note that although the circuit with Tx Configuration 2 may also be controlled to implement the sequential transmission scheme in Configuration 3 or parallel transmission scheme in Configuration 1, we refer Configuration 2 solely for the option of simultaneous transmission.

$$\begin{bmatrix} B_{1x} & B_{1y} & B_{1y} \\ B_{2x} & B_{2y} & B_{2y} \\ B_{3x} & B_{3y} & B_{3y} \end{bmatrix} = \begin{bmatrix} 3zx & 3zy & (3z^2 - d^2) \\ 3yx & (3y^2 - d^2) & 3yz \\ (3x^2 - d^2) & 3xy & 3xz \end{bmatrix}$$

where $C_0 = \mu_o \mu_r NA/(4\pi d^5)$, $\mu_o = 4\pi \times 10^{-7}$ H/m is the magnetic permeability constant, μ_r is the relative permeability of the medium, N is the number of turns, $I_i(t)$ is the current signal flowing through the ith coil, $A = \pi r^2$ is the area of each coil, and r is the radius of each coil, and d is the distance from the origin to the observing point s.

Assume all configurations are well tuned to an operation frequency f_c and the current source is $I_i(t) = \exp\{j2\pi f_0 t + \phi_i\}$. Then the combined magnetic field of Configuration 1 and 2 is the vector sum of the fields of the three coils.

$$\mathbf{B}_{sum} = \mathbf{B}_1 + \mathbf{B}_2 + \mathbf{B}_3$$

Substituting the values of $I_i(t)$ and $\mathbf{B}_i$, the magnitude of the combined magnetic field is

$$B_{sum} = \sqrt{\begin{array}{l} I_1^2(t)C_{11} + I_2^2(t)C_{22} + I_3^2(t)C_{33} + 2I_1(t)I_2(t)C_{12} \\ + 2I_2(t)I_3(t)C_{23} + 2I_3(t)I_1(t)C_{31} \end{array}} \tag{2}$$

$$\begin{aligned} C_{11} &= B_{1x}^2 + B_{1y}^2 + B_{1z}^2 \\ C_{22} &= B_{2x}^2 + B_{2y}^2 + B_{2z}^2 \\ C_{33} &= B_{3x}^2 + B_{3y}^2 + B_{3z}^2 \\ C_{12} &= B_{1x}B_{2x}B_{1y}B_{2y} + B_{1z}B_{2z} \\ C_{23} &= B_{2x}B_{3x} + B_{2y}B_{3y} + B_{2z}B_{3z} \\ C_{31} &= B_{3x}B_{1x} + B_{3y}B_{1y} + B_{3z}B_{1z} \end{aligned}$$

Since Configuration 1 uses a single current source, $I_i(t) = I(t)$, (2) is simplified as

$$B_{c1} = I(t)\sqrt{C4} \tag{3}$$

where $C4 = C_{11} + C_{22} + C_{33} + 2C_{12} + 2C_{23} + 2C_{31}$.

For Configuration 2, the current sources of the three coils can have the same phase or different phases. We studied two options: Option 1 is $\phi_i = 0$ for all i. Then similar to Configuration 1, the magnitude of the combined field strength is then $B_{c2o1} = B_{c1}$. Option 2 is $\phi_1 = 0, \phi_2 = \pi/2$, and $\phi_3 = \pi$. Then the combined field strength is determined by (2)

For Configuration 3, the three magnetic fields are generated in series and will be received at different times. If the received signals are combined by selecting the maximum strength over time, then the equivalent magnetic field strength can be viewed as

$$B_{c3} = \max(B_1, B_2, B_3). \tag{4}$$

where B_1, B_2, and B_3 are the magnitudes of the three transmit coils, respectively.

To illustrate the three configurations, we simulate the magnetic fields using Matlab and the results are shown in Figure 2. The magnetic field is calculated at points around the three coils from $\theta = 0°$ to $\theta = 360°$. Configuration 1 B_{c1} and Configuration 2 Option 1 B_{c2o1} have similar performance, as shown in Figure 2a. They both have oval shaped directionality with maximum strength at 45° and 225°, and minimum strength at 135° and −45°. The maximals and minimals are the results of superimposed fields from different Tx coils adding constructively or destructively at these points. There can also exist points in space where the superposition of the three fields cancels altogether to have a null. The slight difference in B_{c1} and B_{c2o1} is due to the slight phase delay between the three Tx coils in Configuration 1 while Configuration 2 Option 1 has exact the same phase in all three

transmit coils. The directionality in the xy plane is improved in Configuration 2 Option 2 B_{c2o2} by using different current sources with different phases but can still result in null points in a different plane depending on the superposition of the fields.

Configuration 3 results are shown in Figure 2b, where only one coil is transmitting at a time, and the xy plane shows B_1 and B_2 only. It can be seen that magnetic field of each Tx coil is also directional and has minimals and maximals. However, the combined field strength $\max(B_1, B_2, B_3)$, shown as black dots, achieves pretty good strength at all directions, with a slightly reduced strength at $\pm 45^\circ$ and $\pm 135^\circ$. This gives an advantage over the simultaneous transmission to have more coverage points and avoid the probability of getting nulls point in space.

Along with more robustness in space, Configuration 3 also outperforms the other configurations in terms of current consumption. Configuration 2 uses three independent current source and the current consumption is three times of that of Configuration 3. Similarly, Configuration 1 has three coils serially connected, which yields three times of impedance as Configuration 3. Therefore, to produce the same magnetic field, three times as much current is drawn from the source, thus resulting in higher power consumption than Configuration 3.

In the receiver, we assume that the three coils have similar configurations as their Tx counterpart, with the exception that the tuning capacitors are connected with the coils in parallel to achieve the highest induced voltage. The voltage in the receive coils induced by the magnetic field **B** at the receive coil is given by

$$V = B 2\pi f_c N A Q \cos\alpha \tag{5}$$

where B is the magnitude of the magnetic field **B**, A is the area of the receive coil, N is the number of turns of the receive coil, Q is the quality factor of the tuned coil, and α is the angle between the axis of the receive coil and the magnetic field vector **B**.

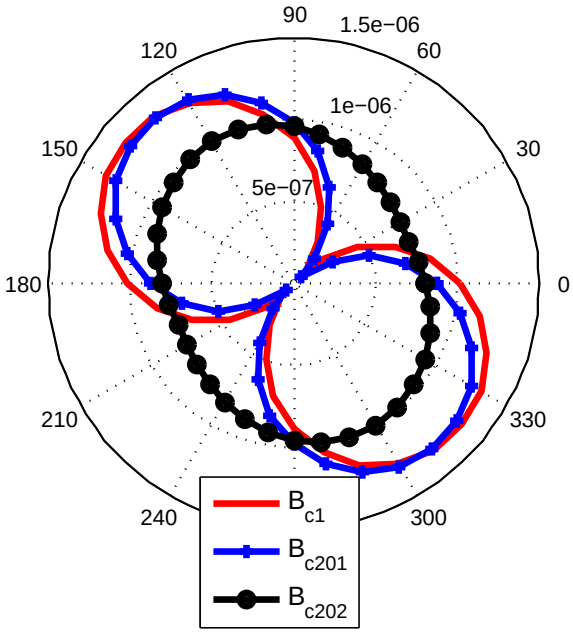

(a) Configurations 1 and 2

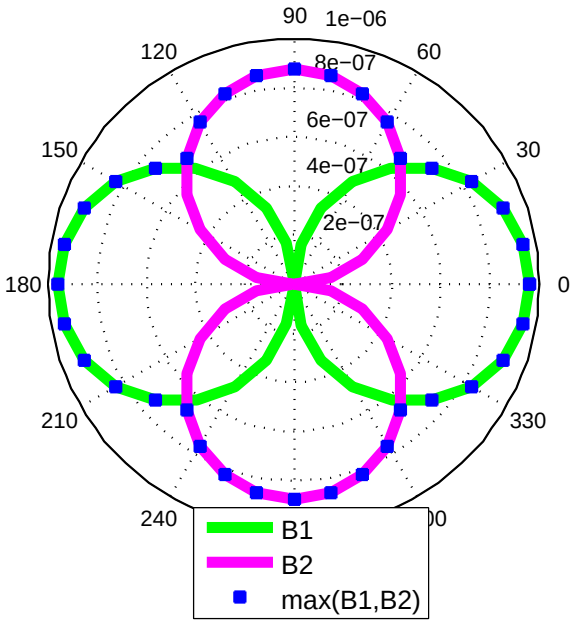

(b) Configuration 3

Figure 2. Magnetic field strength evaluated on the xy plane at $z = 0.5$ m.

We denote the three Rx coils as x,y and z, then α_x, α_y and α_z are the angles between the sum magnetic field vector and the three receive coils, respectively. In Configuration 1 the receive coil induces a single voltage as all the three coils are connected in series. If we define $C_r = 2\pi f_c NAQ$, the induced voltage is given as

$$V_{c1} = B_{c1} C_r [\cos(\alpha_x) + \cos(\alpha_y) + \cos(\alpha_z)] \tag{6}$$

In Configuration 2, each of the three receive coils induces a separate voltage from B_{c2} which is either B_{c2o1} or B_{c2o2} depending on the current source of the two transmit options. The voltages on the three receive coils are given by

$$V_{c2x} = B_{c2} C_r \cos(\alpha_x) \tag{7}$$

$$V_{c2y} = B_{c2} C_r \cos(\alpha_y) \tag{8}$$

$$V_{c2z} = B_{c2} C_r \cos(\alpha_z) \tag{9}$$

In Configuration 3, the receiver has the advantage to select the maximum of the three individual transmitted fields in B_{c3}.

$$V_{c3,i} = B_i C_r \max_{x,y,z} [\cos(\alpha_{i,x}), \cos(\alpha_{i,y}), \cos(\alpha_{i,z})] \tag{10}$$

$$V_{c3} = \max_i (V_{c3,i} i = 1, 2, 3) \tag{11}$$

The receiver then choose the strongest of $V_{c3,i}$ for future communication needs unless the sensor node has moved.

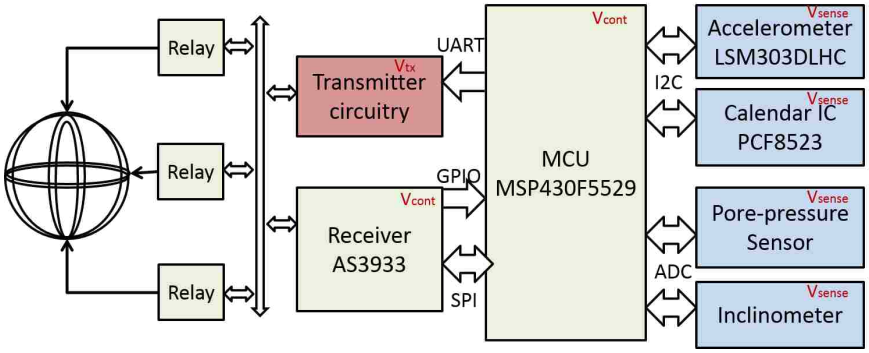

Figure 3. Block Diagram of the low-cost sensor node with MI communication and sensing capabilities

3. DESIGN AND IMPLEMENTATION OF SENSOR NODES

Based on the analysis in Section 2, we chose Configuration 3 for the design and implementation of our underwater and underground sensor nodes. The design goals are to achieve low power, low cost, sensing capability, good omni-directionality for localization, and robustness in communication and networking capability. This section describes the hardware and software design and implementation of the sensor nodes.

3.1. Hardware Implementation. The multi-coil transceiver hardware architecture is shown in Fig. 5, where most of the components are Commercial Off The shelf (COTS). The main component is the micro-controller unit (MCU) which is the brain of the system. We have selected Texas Instruments MSP430F5529 for its low-power, many Analog to Digital Converter (ADC) channels, and amber I/O ports. The digital sensor chips include accelerometer and calendar IC, which are connected to the micro-controller via I2C bus. The analog sensing devices include the pore pressure sensor and inclinometer which are connected to the MCU via the on-chip ADC interfaces. The receiver design uses a watch dog receiver AS3933 which uses the SPI serial bus for control commands and uses the general purpose input/output pins (GPIO) for data communications. The transmitter ATA5276 is controlled by the MCU through Universal Asynchronous Receive and Transmit (UART) port.

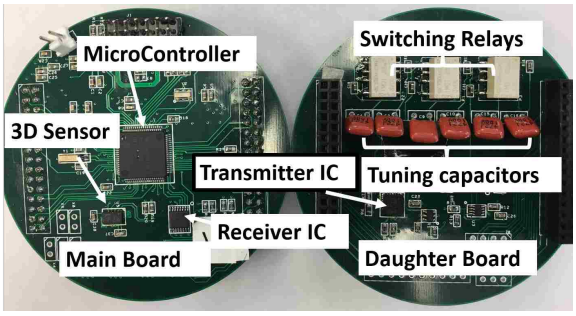

Figure 4. PCB of the sensor node

The three coils in spherical configuration, along with their matched tuning capacitors, are connected to the transmitter or receiver circuitry through relays. All three coils independently receive the transmitted signals which are fed to the three input ports of the AS3933 simultaneously. The AS3933 uses selection combining which chooses the signal with the highest received signal strength (RSS) measure and pass it to the micro-controller. The Printed Circuit Board is shown in Fig. 4, where the two circular boards are joined by connectors and can be debugged separately. The main board contains the MCU, sensors, and the receiver circuitry. The daughter board contains the tuning relays, tuning capacitors, and the transmitter. The diameter of the boards is 7.5 cm, and the thickness of the two fully assembled boards is 2 cm.

The sensor node runs on an external battery power supply of 3.6 V which is the only power source. The MCU and the receiver AS3933 requires a 3.3 V, the analog sensors require ±5 V, and the transmitter ATA5276 requires +12 V. The power is distributed to the different components via three power levels V_cont, V_sense and V_tx, as shown in Figure 5. V_cont is the regulated $3.3V$ and is supplied to the components that have to run continuously. V_sense and V_tx are supplied to the sensors and the transmitter circuitry when the sensor node has to sense or transmit data. The MCU controls two switches to turn on the two powers independently when they are needed. The transmitter power has to be boosted from the 3.6 V external battery or the V_cont. The booster IC used is ADP1613SMSOP8.

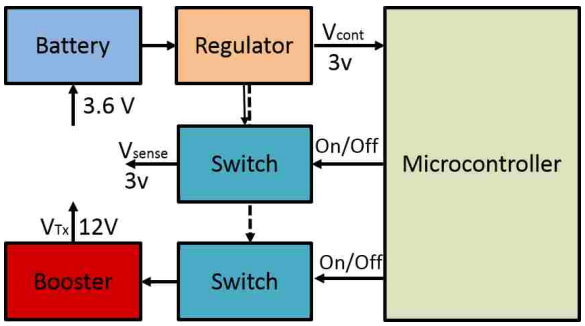

Figure 5. Block Diagram of Power Control

The low power watchdog receiver AS3933 provides excellent features: it records the RSSI of the incoming signals on all three coils with a 5 bits quantization; it allows to decode manchester encoded data to improve bit error performance, and it supports On-Off keying (OOk) demodulation. The receive sensitivity of AS3933 is 80 μV and its idle mode power consumption is as low as 12 μA. AS3933 also provides 32 bit ID detection and carrier frequency detection which makes it perfectly suited for sensor network protocols such as CSMA (Carrier Sensing Multiple Access).

The transmitter ATA5276 is originally designed for Tire Pressure Management Systems (TPMS) and can operate in the 100 kHz – 150 kHz frequency band. The IC drives the LC antenna tank to the desired frequency and the transmit signal is sent from the micro-controller through the UART interface. The transmitter has a maximum output current of 1 A.

The three coils have the same radius of 0.11 m and the number of turns is 29. The coil acts as an inductor which form a R-L-C resonance circuit with the tuning capacitor. The equivalent transceiver circuit is shown in Figure 6, where the tuning capacitor is connected in series with the coil at the transmitter achieve a small impedance which in turn yields a high transmit current on the coil. On the other hand, the receiver requires high impedance to respond to the small changes in magnetic flux passing through the coil, so the tuning capacitor is connected in parallel with the coil. Since the same coil and tuning capacitor

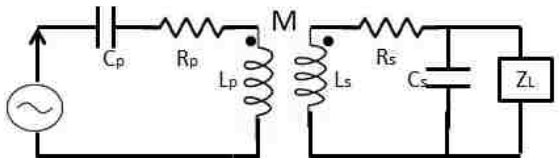

Figure 6. Equivalent series and parallel RLC circuits for transmit and receive configurations. respectively. The mutual inductance M between the transmit and receive coils is linearly proportional to the magnetic field strength B_i.

Table 1. Low Power Modes of Micro-controller

Power Mode	Max Current	Peripherals Disabled	Peripherals Enabled
LPM0	95 (μA)	CPU, MCLK	ACLK, SMCLK & FLL loop
LPM1	85 (μA)	CPU, MCLK & FLL	ACLK & SMCLK
LPM2	18 (μA)	CPU, MCLK & FLL loop	ACLK
LPM3	12 (μA)	CPU, MCLK & FLL loop	ACLK
LPM4	8.5 (μA)	CPU, MCLK, FLL loop & ACLK	None

are used for both transmit and receive circuitries, the two configurations are switched via a relay which is controlled by the micro-controller. By default, the relay connects the receiver configuration and, when the node needs to transmit data, the micro-controller switches the relay to the series configuration and then returns to parallel configuration after the transmission.

The relationship between the operation frequency, capacitance and inductance for antenna tuning is $F = 1/(2\pi\sqrt{LC})$. The resonant frequency has to be accurately tuned for better performance. To tune the coils to operate at 125 kHz, we used 1% 4.78 nF capacitors since the measured inductance was 340 μH.

3.2. Software Implementation. The sensor node is programmed using the code composer studio (CCS v5.5). To lower the power consumption, the sensor node is kept in the idle mode for most of the time. The MCU provide five low power modes. Each low

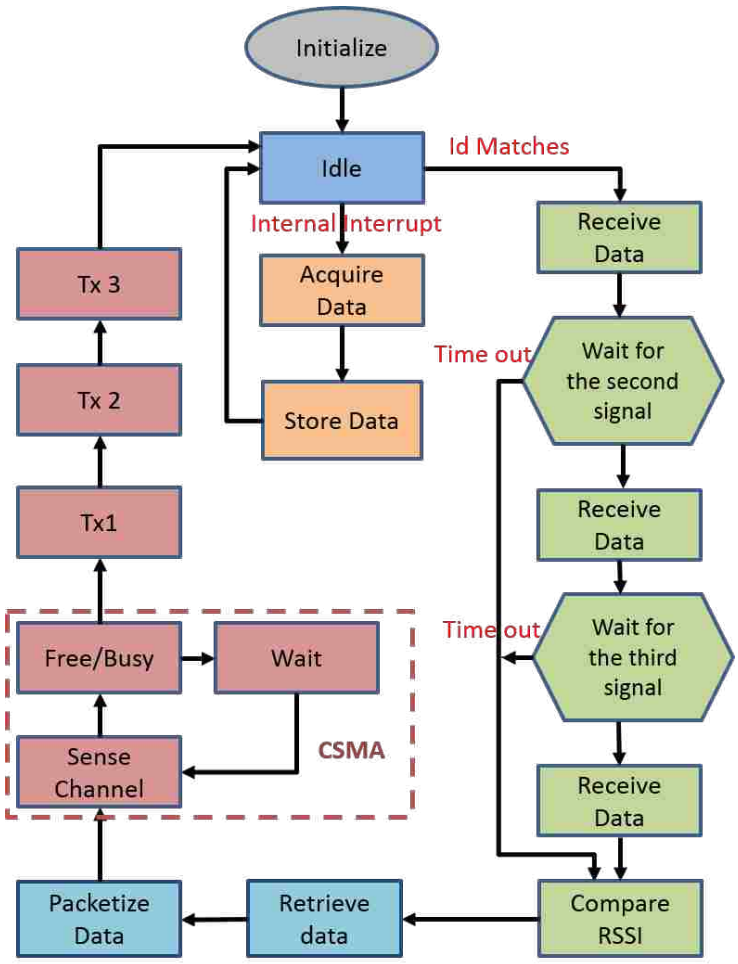

Figure 7. Flow chart diagram of sensor node implementation

power mode consumes current depending on the peripherals enabled and disabled as shown in the Table 1. We choose LPM3 mode due to need of asynchronous clock (ACLK) for the timer being used.

Figure 7 shows the software implementation of the sensor node. The node starts with the initialization of the clock, variables and peripherals and enters into an idle state. The node remains in the idle state until one of the two interrupt occurs: signal received with matching the node's unique ID or the internal interrupt. The internal interrupt occurs due

to a timer which is set to run until a predefined interval t_{sense}. Each time the timer reaches the time = t_{sense}, the sensor node wakes up, acquires data from the interfaced sensors and stores the data in the memory. The node then returns to the idle state.

In idle state, if a signal is detected, the node will compare the target ID with its own unique ID in the received frame. If the ID matches the node enters the receive flow graph. The node receives the incoming data, decodes the packet and records RSSI. Since we are using Configuration 3, the node expects to receive the signal transmitted at second and third time slots. It is possible that the sensor node is placed in a location where all the three coils of the Tx node can not reach the Rx node, so a timer is used to avoid waiting for long intervals. Once the data is received through the coils, the sensor node compares the RSSI, look for the strongest Tx coil and retrieve the sensor's data from the memory. The data is then feed to the next block where the data is packetized into transmitted frame.

Figure 8 shows the transmitted frame which starts with one byte carrier and one byte preamble followed by the four byte destination/target ID. The receive sensor node is looking for this four byte target ID and upon matching this ID, the receive sensor node wakes up the MCU and start decoding the rest of the packet. The rest of the frame consists of the sender node and coil information along with a command or sensors data followed by one byte EOF to indicate the end of the frame.

Once the transmit packet is ready, the sensor node uses CSMA implementation to avoid collision of transmitted packets. The sensor node senses the channel and wait if a transmission is detected. After a transmit packet interval time, the sensor node senses the channel again and if no transmission is detected, the sensor node transmits the data out using the three coils sequentially and goes back to the idle state.

Carrier	Preamble	Target ID	Sender Node ID	Coil ID	Sensor Data	EOF
1 byte	1 byte	4 bytes	4 bytes	1 byte	8 bytes	1 byte

Figure 8. Transmitted Data frame

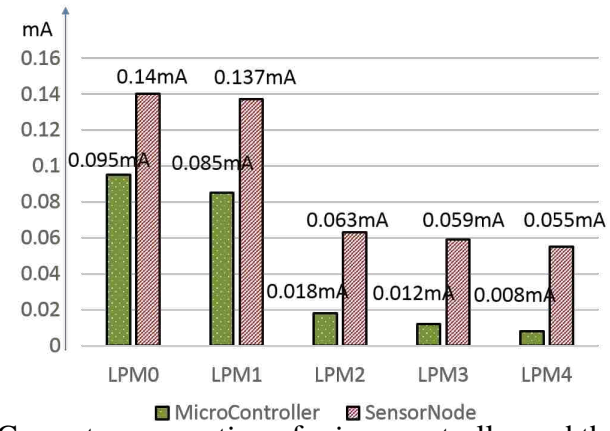

Figure 9. Current consumption of micro-controller and the sensor node

4. PERFORMANCE EVALUATION

We now evaluate our MI sensor node performance. We calculate current consumption of the sensor nodes in different working modes, show the directivity pattern and perform range experiments to determine the maximum distance with our sensor node. We next explain these tests

4.1. Power and Energy Consumption. Figure 9 shows the current consumption of the MCU and the sensor node in the various available low power modes. The results show that the sensor node consumes an average of 45μA other than the MCU current consumption. We then compute the current consumption in the three main operating modes: idle/sleep mode, receive mode and transmit mode as shown in Table 2. We perform the same measurements with five different sets of sensor nodes to verify the robustness and consistency of the sensor nodes.

The sensor node uses LPM3 for the sleep mode operation. To measure the current in idle/sleep mode the node is programmed to remain in the idle mode and the average current consumption is recorded as 60μA. To measure the current in receive mode, another sensor node is set to transmit data to let our measuring sensor node receive data. A total of 200 byte frame (1.6 second long) is transmitted from the other sensor node to make sure the current is measured over a fair amount of time for receive mode. The average current in the receive

mode is recorded as 0.49mA. For the transmit mode, the sensor node is programmed to keep transmitting long bytes of data. Since the data is Manchester encoded, any sequence of data will be represented by an equal amount of zeros and ones resulting in transmitting half of the time. After a repetitive measurements on different sensor node the transmit mode current is recorded as 253mA.

Table 2. Current consumption in operating modes

	Sleep Mode	Receive Mode	Transmit Mode
Node 1	0.074 μA	0.53 m A	277 m A
Node 2	0.067 μA	0.50 m A	277 m A
Node 3	0.043 μA	0.49 m A	225 m A
Node 4	0.044 μA	0.42 m A	230 m A
Node 5	0.073 μA	0.52 m A	260 m A

Based on the current consumption in different modes, we calculate the life time the sensor node can achieve in a given wireless sensor network application by following equations by using

$$I_{avg} = \sum I_{mode} * t_{mode}$$

$$T_{life} = C_{battery} / I_{avg}$$

where $C_{battery}$ is the battery capacity, I_{avg} is the average current per hour, I_{mode} is the current consumed in the mode and t_{mode} is the time it remains in the mode in a given hour. The modes are sleep, receive and transmit. With the given battery of 19 Ampere-Hours capacity, the calculations are shows in Figure 10 The lifetime is calculated with a network size of 10, 50 and 100 nodes. The number of transmission in a given hour is also considered. The calculation shows that the sensor node can survive about 5 years for a high traffic and a dense network of 100 nodes. For a low traffic and a less dense network the sensor node can survive for 28 years.

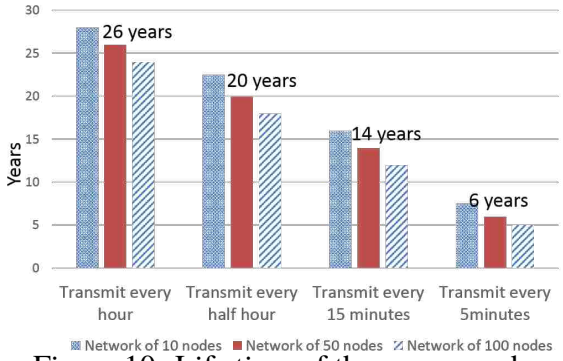

Figure 10. Life time of the sensor node

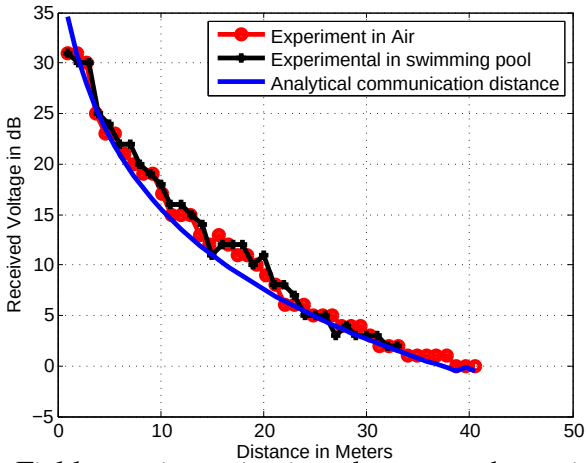

Figure 11. Field experiment in air and water vs theoretical results

4.2. Communication Distance. We now present the range testing of our sensor nodes. We present the theoretical range with our current system parameters and verify with our experimental range experiments. We perform the range tests both in air and water to compare the air and water performance of the MI sensor node. The in-air tests were conducted at a drive way and parking lot near HyPoint Industrial Park, Rolla, MO while the underwater tests were conducted in a swimming pool of the university.

To perform the range experiment we use two sensor nodes. Each sensor node is interfaced with the three dimensional coil and can act as both transmit and receive node . For the purpose of range experiments we program one node to Tx and the other node to Rx. The Tx node transmits a wakeup command to the Rx node. The Rx node starts with the sleep mode and upon receiving the wakeup command, wakes up and records the RSSI. The Rx and Tx nodes are placed on the same axis aligned to each other and after recording the RSSI value, the distance is increased between them until the Rx node stops waking up. For underwater range experiment, we use the plastic buckets to house the sensor boards and coils for easy placement when performed experiments in water. We also use some weights inside the bucket to allow the buckets to sink in water.

Figure 11 shows the theoretical and experimental received voltage where x-axis is distance in meters and y-axis is the received voltage in decibels. Similar RSSI values can be seen for in-air and underwater results. The RSSI values for the water are only recorded until the length of the swimming pool, that is 30m. The maximum range for the current version of MI sensor node is recorded as 38m. To compare with the field experiments we find the analytical range of the sensor node using the transmit magnetic field and received voltage equations (1) and (5) where $N = 29$, $I = 0.8A$, $r = 0.104$m, $f = 125$ kHz.

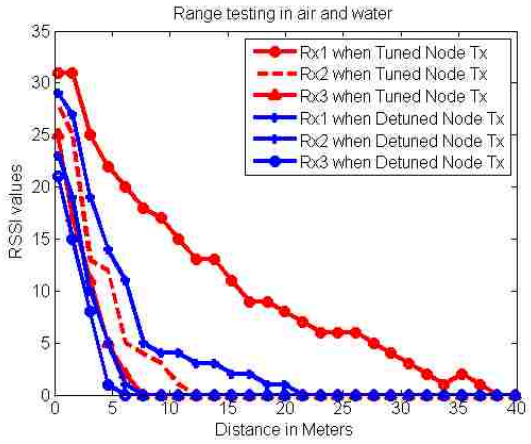

Figure 12. Effect of Detuning on Performance

Effect of Tuning/Detuning on Performance Figure 12 compares the range results by using a tuned and detuned sensor nodes. The purpose of the experiment is to show the effect of detuning on the performance of the sensor node communication. It can be seen that when the coil is detuned the performance degrades alot and limit the communication distance. Thus, tight tuning of the sensor node to the desired frequency is very important.

4.3. Directivity Pattern. The primarily purpose of the three coil design is to improve the directivity pattern that can increase the robustness of the senor node when deployed in a practical application. To verify the importance of using multi coil design, we perform the measurements using both one and three coil and then compare the results.

The experiment is performed using two sets of coils: one node is programmed to transmit a 20 byte sequence and the other node is placed in the vicinity to receive the signal. The receive node is connected to the oscilloscope to record the strength of the signal. The signal voltage is recorded after each rotation of 15° until 180° as the measurements repeats after that. The test is repeated for the four possible combinations of one and three coil: one coil Tx vs One coil Rx, one coil Tx vs three coil Rx, three coil Tx vs one coil Rx and three coil Tx vs three coil Rx as shown in Figure 13.

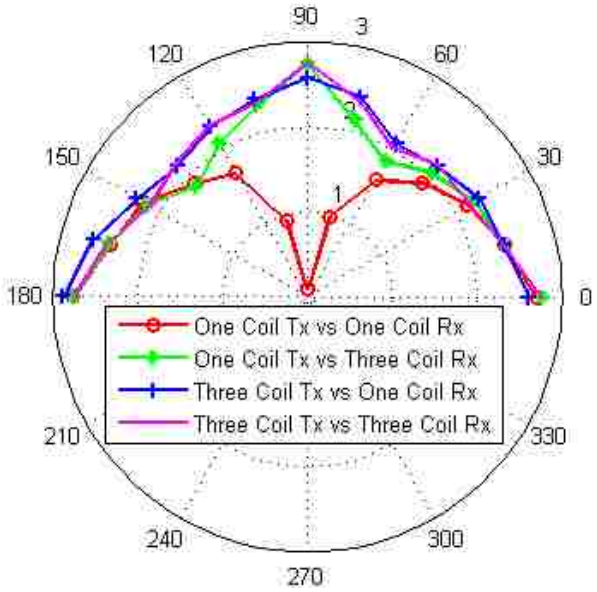

Figure 13. Directivity patterns of one and multi coil sensor node. The 3-coil config yielded an omni-directional pattern, while the 1-coil config was directional.

Figure 13 shows the directional nature using single coils at Tx and Rx. One coil Tx vs one coil Rx performs the worst with orientation. Using one coil Tx vs one coil Rx performs almost yields no communication at 90°. On the other hand using three coil at either Tx or Rx, improve the communication robustness as one of the three coils gets aligned after 90° of rotation. Using three coils at both Tx and Rx further improve the communication robustness and performance. Deployed in a practical application, one can not guarantee a sensor node to maintain a specific rotation, thus use of three coil sensor node is important.

To further illustrate the advantage of using three coils for omni-directionality, We use EMC Studio [1] to create the three dimensional model as shown in Figure 14a and run simulations. The Tx and Rx node are separated by a distance of 1 meter or 50 meters. Both the Tx and Rx nodes are randomly rotated and the received strength on each coil is shown in Figure 14. It can be seen that while individual readings from the three RX-coils vary wildly and the difference can be as large as 50 dB, the maximum value of the three Rx coils

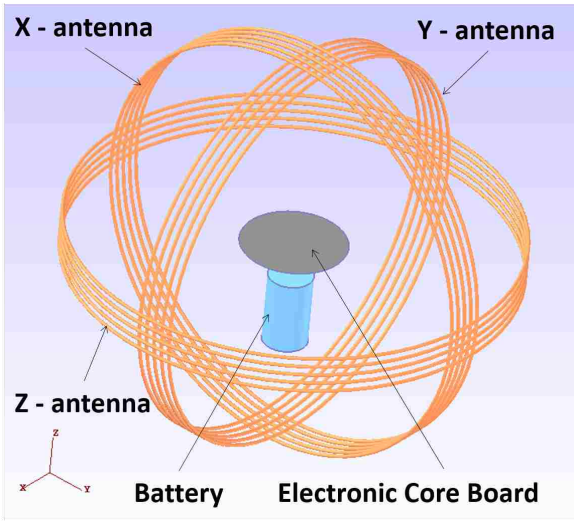

(a) RSSI with the three coils at 1m and 50m

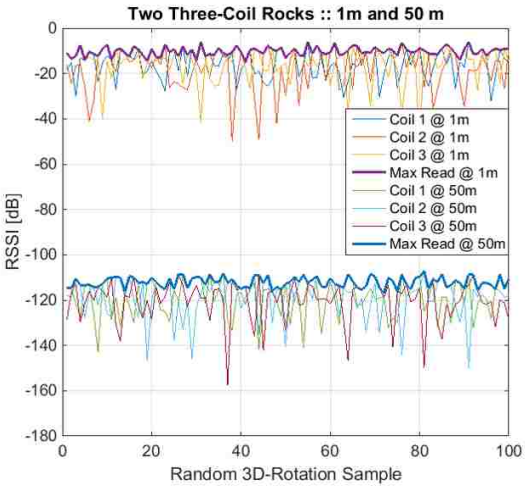

(b) RSSI of three Rx coils at 1 m and 50 m

Figure 14. Directivity test using EMC Studio Simulations

stays rather constant and the difference is in the range of 5 dB. This simulation validated the near omni-directional receiving properties of using three coils and the results confirmed with the field experiments.

5. CONCLUSION

A low-cost and low power multi-coil MI communication system has been presented for underground and underwater wireless sensor network applications. Three different transmission configurations have been investigated to choose the optimal configuration. The hardware and software implementation have been explained in detail and field tests have been performed to demonstrate the promising communication range and robust performance of the sensor node.

REFERENCES

[1] URL https://www.emcos.com/?products=emc-studio.

[2] *FreeLinc Near-Field Magnetic Induction Technology*. URL http://www.freelinc.com/downloads/FreeLinc/20NFMI/20White/20Paper.pdf.

[3] Johnson I Agbinya. Investigation of near field inductive communication system models, channels and experiments.(report). *Progress In Electromagnetics Research B*, 49: 129–153, April 2013. doi: doi:10.2528/PIERB12120512.

[4] N. Ahmed, J. Hoyt, A. Radchenko, D. Pommerenke, and Yahong Rosa Zheng. A multi-coil magneto-inductive transceiver for low-cost wireless sensor networks. In *Proc. Underwater Communications Networking Conf.*, pages 1–6, September 2014. URL http://ucomms.net/.

[5] I. F. Akyildiz, P. Wang, and Z. Sun. Realizing underwater communication through magnetic induction. *IEEE Communications Magazine*, 53(11):42–48, November 2015. ISSN 0163-6804. doi: 10.1109/MCOM.2015.7321970.

[6] Shlomi Arnon and Debbie Kedar. Non-line-of-sight underwater optical wireless communication network. *J. Opt. Soc. Am. A*, 26(3):530–539, March 2009. doi: 10.1364/JOSAA.26.000530. URL http://josaa.osa.org/abstract.cfm?URI=josaa-26-3-530.

[7] R. Carta, M. Sfakiotakis, N. Pateromichelakis, D. ThonÃĺ, J.and Tsakiris, and R. Puers. A multi-coil inductive powering system for an endoscopic capsule with vibratory actuation. 172(1):253–258, 2011. doi: 10.1016/j.sna.2011.03.036.

[8] J.A. Catipovic. Performance limitations in underwater acoustic telemetry. *IEEE J. Ocean. Eng.*, 15(3):205–216, July 1990. doi: 10.1109/48.107149.

[9] X. Che, I. Wells, G. Dickers, P. Kear, and X. Gong. Re-evaluation of rf electromagnetic communication in underwater sensor networks. *IEEE Commun. Mag.*, 48(12):143–151, December 2010. ISSN 0163-6804. doi: 10.1109/MCOM.2010.5673085.

[10] Marco Dionigi, Guido De Angelis, Antonio Moschitta, Mauro Mongiardo, and Paolo Carbone. A simple ranging system based on mutually coupled resonating circuits. *IEEE trans. Instrum. Measure*, 63(5), 2014.

[11] B. Gulbahar and O.B. Akan. A communication theoretical modeling and analysis of underwater magneto-inductive wireless channels. *IEEE Trans. Wireless Commun.*, 11 (9):3326–3334, September 2012. ISSN 1536-1276. doi: 10.1109/TWC.2012.070912.111943.

[12] O. Jonah, S.V. Georgakopoulos, and M.M. Tentzeris. Orientation insensitive power transfer by magnetic resonance for mobile devices. In *Wireless Power Transfer (WPT), 2013 IEEE*, pages 5–8, May 2013. doi: 10.1109/WPT.2013.6556868.

[13] M. Manteghi and A.A.Y. Ibraheem. On the study of the near-fields of electric and magnetic small antennas in lossy media. *IEEE Trans. Antennas Propag.*, 62(12): 6491–6495, Dec 2014. ISSN 0018-926X. doi: 10.1109/TAP.2014.2359499.

[14] Andrew Markham, N. Trigoni, D.W. Macdonald, and S.A. Ellwood. Underground localization in 3-d using magneto-inductive tracking. *IEEE Sensors J.*, 12(6):1809–1816, June 2012. ISSN 1530-437X. doi: 10.1109/JSEN.2011.2178064.

[15] S.A. Meybodi, M. Dohler, A.N. Askarpour, J. Bendtsen, and J.D. Nielsen. The feasibility of communication among pumps in a district heating system. *IEEE Antennas Propagat. Mag.*, 55(3):118–134, June 2013. ISSN 1045-9243. doi: 10.1109/MAP.2013.6586631.

[16] H. Nguyen, J.I. Agbinya, and J. Devlin. FPGA-based implementation of multiple modes in near field inductive communication using frequency splitting and MIMO configuration. *IEEE Trans. Circuits Syst. I, Reg. Papers*, 62(1):302–310, Jan 2015. ISSN 1549-8328. doi: 10.1109/TCSI.2014.2359716.

[17] Andriy Radchenko, David Pommerenke, Genda Chen, Pratik Maheshwari, Satyajeet Shinde, Viswa Pilla, and Yahong R. Zheng. Real time bridge scour monitoring with magneto-inductive field coupling. volume 8692, pages 86922A–86922A–15, April 2013. doi: 10.1117/12.2009002. URL `http://dx.doi.org/10.1117/12.2009002`.

[18] A. Reza and J. Harms. Robust grid-based deployment schemes for underwater optical sensor networks. In *IEEE 34th Conf. LCN 2009*, pages 641–648, October 2009. doi: 10.1109/LCN.2009.5355122.

[19] A. Sheinker, B. Ginzburg, N. Salomonski, L. Frumkis, and B.-Z. Kaplan. Localization in 3-D using beacons of low frequency magnetic field. *IEEE Trans. Instrum. Meas.*, 62(12):3194–3201, Dec 2013. ISSN 0018-9456. doi: 10.1109/TIM.2013.2270919.

[20] J.J. Sojdehei, P.N. Wrathall, and D.F. Dinn. Magneto-inductive (mi) communications. In *MTS/IEEE OCEANS Conf.*, volume 1, pages 513–519, November 2001. doi: 10.1109/OCEANS.2001.968775.

[21] M. Stojanovic and J. Preisig. Underwater acoustic communication channels: Propagation models and statistical characterization. *IEEE Commun. Mag.*, 47(1):84–89, January 2009. ISSN 0163-6804. doi: 10.1109/MCOM.2009.4752682.

[22] Zhi Sun and I.F. Akyildiz. Magnetic induction communications for wireless underground sensor networks. *IEEE Trans. Antennas Propag.*, 58(7):2426–2435, July 2010. ISSN 0018-926X. doi: 10.1109/TAP.2010.2048858.

[23] Syms, Young, and L Solymar. Low-loss magneto-inductive waveguides. *J. Phys. D: Appl. Phys.*, 39(18):3945–3951, 2006. doi: doi:10.1088/0022-3727/39/18/004. URL `http://stacks.iop.org/0022-3727/39/i=18/a=004`.

[24] Dongyang Wang, Yongxin Zhu, Hongliang Guo, Xinen Zhu, Tingting Mo, and Qiyu Huang. Enabling multi-angle wireless power transmission via magnetic resonant coupling. In *Computing and Convergence Technology (ICCCT), 2012 7th International Conference on*, pages 1395–1400, Dec 2012.

[25] H. Wegleiter, B. Schweighofer, C. Deinhammer, G. Holler, and P. Fulmek. Automatic antenna tuning unit to improve rfid system performance. *IEEE Trans. Instrum. Meas.*, 60(8):2797–2803, Aug 2011. ISSN 0018-9456. doi: 10.1109/TIM.2011.2122390.

[26] Yahong Rosa Zheng, Zengli Yang, Jinxing Hao, and Peng Han. Hardware implementation of underwater acoustic localization system for bridge scour monitoring. In *Proc. MTS/IEEE Oceans*, pages 1–6, September 2013.

[27] Zhong Zhou, Jun-Hong Cui, and Shengli Zhou. Efficient localization for large-scale underwater sensor networks. *Ad Hoc Networks*, 8(3):267–279, 2010. doi: doi:10.1016/j.adhoc.2009.08.005.

II. THEORETICAL MODELING OF MULTI-COIL CHANNELS IN NEAR FIELD MAGNETO-INDUCTIVE COMMUNICATION

Niaz Ahmed, Y. Rosa Zheng, David Pommerenke

Department of Electrical & Computer Engineering

Missouri University of Science and Technology, Rolla, MO 65409, USA.

(email:{namn3, zhengyr}@mst.edu)

ABSTRACT

This paper presents theoretical modeling and circuit analysis of magneto-inductive communication channels where receivers use multiple coils to improve the spatial sensitivity patterns and communication range. The mutual coupling among the multi-coils at receiver and between transmit and receive coils is derived for general configurations in 3D space. The equivalent circuit of induced voltage for receive coils is analyzed which provides a guide for the design of matching circuits for optimal performance. The methodology developed in this paper can also be applied to other sensor network scenarios where MI communications are used.

1. INTRODUCTION

Unlike RF communications that relies on electromagnetic wave propagation, Near Field Communication (NFC) is achieved by magnetic field induction/resonance between transmit and receive coils at distances much less than a wavelength of the carrier frequency. Recent applications of NFC include nearfield touchless entry [35, 29, 37] and RF identification (RFID) [42, 28]. The magneto inductive communication (MI) has also been used as an alternative to acoustic communications for underground and underwater applications [41, 39, 33, 40, 34, 30].

Recently, researchers have put efforts to study, analyze and model the MI channel. The related literature involve study of magnetic field of a current carrying coil, amount of mutual inductance among coupled coils and equivalent circuit analysis of the the transformer model. Significant amount of work has been done by Babic et al. in deriving expressions for mutual inductance among resonant coils arbitrarily placed in three dimension space[31]. Equivalent circuit analysis have also been performed and presented in[32, 38]. In another work, Gulbahar et al modeled dense underwater MI channels [34] with closely placed transmitters and receivers. Our work builds on top of these efforts to model and analyze a multi coil receiver system.

This paper presents theoretical modeling of mutual inductance of the transmit and receive coils and by performing equivalent circuit analysis to derive expressions for the induced voltage. Two types of orthogonal configuration of the three coils at the receiver side are discussed: spherical configuration where all the three coils are centered at the same point such that the mutual inductances of the three coils are independent, and the three coils arranged on three sides of a cubic with different centers which caused interfering fields and detuning at the operating frequency. It is shown that the spherical configuration enables the coils to be tuned to the same resonant frequency and induces more voltage than cubical configuration.

2. MUTUAL INDUCTANCE OF RESONANT COILS

Similar to Radio Frequency (RF) electro-magnetic waves, MI communication systems employ alternating Electric (**E**) and Magnetic (**B**) fields as the data carrier [36]. The **E** and **B** fields generated by alternating electrical current in a transmit antenna coil can be modeled by Maxwell equations, and their field strengths decay with the distance r from the transmit current source. Let the operating frequency of the current source be $\omega = 2\pi f$. Then the wavenumber is $\kappa = \omega/v$ with v being the wave propagation speed in the medium. The region that $r\kappa \ll 1$ is called static field, in which the **E** and **B** fields attenuate at a rate

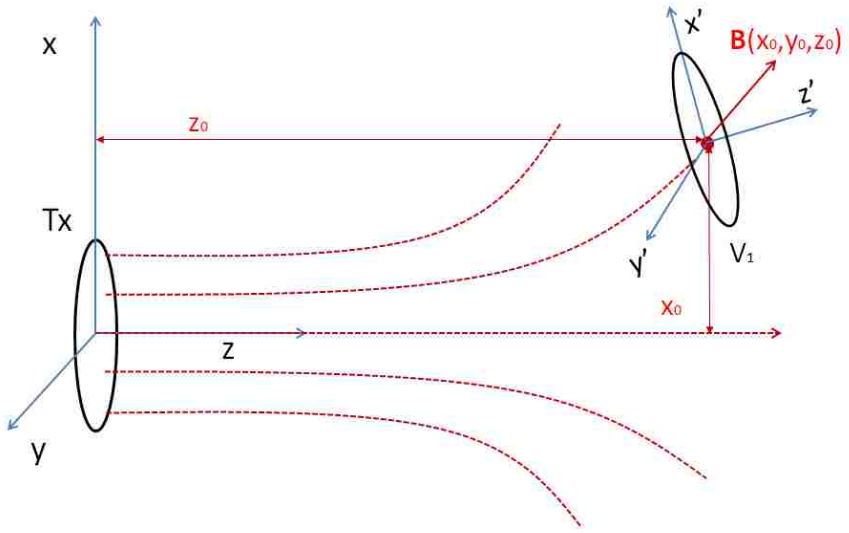

Figure 1. Coordinate system of the transmit coil and receive coil.

of $1/r^3$. If $r\kappa \gg 1$, then the field is called radiation field and the field strength decays at a rate of $1/r$. In between, the field is called quasi-static field and the strength decays at $1/r^2$. Unlike RF communication systems that operate in the radiation field, MI communication systems operate in static or quasi-static fields by using low frequency and/or low power.

To model the MI communication channels, the mutual inductance of the transmit and receive coil is analyzed here. Figure 1 shows the tx-rx MI system model, where a transmit coil is located at the origin and on the $x-y$ plane of the $x-y-z$ coordinate system. On the receive side, the coil is centered at point (x_0, y_0, z_0), and aligned on the $x'-y'$. Denote the normal vectors of the rx coil as $\hat{\mathbf{z}}'$, $\hat{\mathbf{y}}'$, and $\hat{\mathbf{x}}'$, respectively, since these vectors align with z', y', and x' axes, respectively. Let θ_i be the "in-plane tilt angle" of the ith normal vector around axis x, and ψ_i be the rotation angle of the ith normal vector around axis z. The parameters (x_0, y_0, z_0) and (θ_i, ψ_i) describe the lateral and angular displacement between the transmit and receive coils.

Although the Finite Element Method (FEM) and Boundary Element Method (BEM) are commonly used for calculating the mutual inductance of a pair of transmit and receive coils with arbitrary displacement parameters, a fast-convergent formulas is given by [31] as

$$M(R_i,\theta,\psi)=\frac{\mu_0 N_t N_r R_i}{\pi}\int_0^{2\pi}\frac{(p_1\cos\varphi+p_2\sin\varphi+p_3)\Psi(m)}{\sqrt{mU_0^3}}d\varphi \tag{1}$$

where μ_0 is the magnetic permeability constant, N_t and N_r are the numbers of turns of the transmit and receive coils, respectively, R_i is the radius of the ith receive coil, and other definitions are

$$\begin{aligned}
&a=\sin\theta\sin\psi,\quad b=-\sin\theta\cos\psi,\quad c=\cos\theta,\\
&\alpha=\frac{x_0}{R_t},\quad \beta=\frac{y_0}{R_t},\quad \gamma=\frac{z_0}{R_t},\quad \delta_i=\frac{R_i}{R_t},\\
&l=\sqrt{a^2+c^2},\quad L=\sqrt{a^2+b^2+c^2},\\
&p_1=\frac{\beta c}{l},\quad p_2=\frac{\alpha l^2+\beta ab}{lL},\quad p_3=\frac{\delta_i c}{L},\\
&p_4=p_6+\gamma bc/(lL),\quad p_5=p_7-\gamma a/l,\\
&p_6=(\alpha ab-\beta l^2)/(lL),\quad p_7=\alpha c/l,\\
&A_0=1+\alpha^2+\beta^2+\gamma^2+\delta_i^2\mp 2\delta_i(p_4\cos\varphi+p_5\sin\varphi),\\
&U_0^2=\delta_i\left[\left(1-\frac{b^2c^2}{l^2L^2}\right)\cos^2\varphi+\frac{c^2}{l^2}\sin^2\varphi+\frac{abc}{l^2L}\sin(2\varphi)\right]\\
&\qquad+\alpha^2+\beta^2\mp 2\delta_i\left(p_6\cos\varphi+p_7\sin\varphi\right),\\
&m=\frac{4U_0}{A_0+2U_0},\quad \Psi(m)=\left(1-\frac{m}{2}\right)K(m)-E(m).
\end{aligned} \tag{2}$$

and where R_t is the radius of the transmit coil, $K(m)$ and $E(m)$ are the complete elliptic integrals of the first and second kind, respectively, defined as

$$K(m)=\int_0^{\pi/2}\frac{d\alpha}{\sqrt{1-m\sin^2\alpha}} \tag{3}$$

and

$$E(m) = \int_0^{\pi/2} \sqrt{1 - m \sin^2 \alpha} d\alpha \tag{4}$$

For the special case that $a = 0, c = 0$ and $l \to 0$, some of the parameters in (2) are simplified into

$$\begin{aligned} &p_1 = 0, \quad p_2 = \mp\beta \mathrm{sgn}(b), \quad p_3 = 0, \\ &p_4 = \mp\alpha \mathrm{sgn}(b), \quad p_5 = \pm\gamma, \\ &U_0 = \alpha^2 + \beta^2 + \delta_i^2 \cos^2 \varphi \mp 2\alpha\delta_i \mathrm{sgn}(b) \cos \varphi. \end{aligned} \tag{5}$$

For the special case of $x_0 = 0, y_0 = 0$, the transmit and receive coils are parallel, (1) will experience numerical instability. A small offset ϵ shall be added to the center coordinates to mitigate the problem.

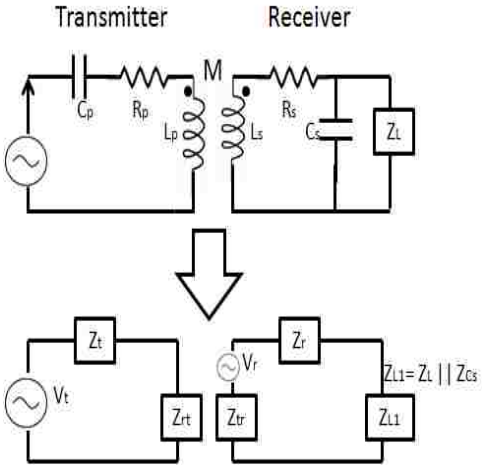

Figure 2. Equivalent circuit and transformer model of Tx and Rx coupled coil

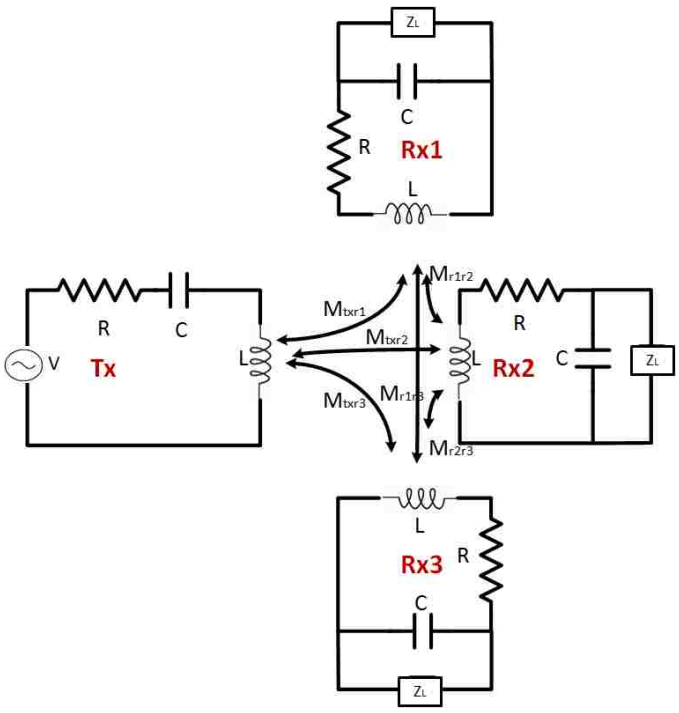

Figure 3. Tx and Multi coil Rx with mutual coupling

3. EQUIVALENT CIRCUIT ANALYSIS OF 3D MULTI COIL MODEL

Figure 2 shows transformer model and equivalent circuit of two coupled coils where M is the mutual induction of the transmitter coil and receiver coil, V_r is the voltage induced at the receiver side, V_t is the voltage of transmitter battery. Z_{rt} is the effect of receiver coil on transmit coil and Z_{tr} is the effect of transmitter coil on receive coil. Similarly Z_t and Z_r are the self impedances of transmit and receive coils.

It can also be noted that since the transmitter needs to transmit a strong signal, the impedance needs to be small; this is why the tuning capacitor is used in series with the coil. On the other hand, the transceiver requires high impedance to respond to the slight change produced by magnetic flux passing through it, so the tuning capacitor is used in parallel with the coil.

For a given Tx-Rx separation, the maximum voltage output is obtained when the receive coil is aligned with the transmit coil. We see in [30] that using one coil at the receiver gives directional communication and using three coil at the receiver makes the communication more robust and omni-directional.

Figure 3 shows the transformer model of the transmit coil and multi-coil receiver. The figure shows all the possible combinations of the mutual coupling among all the coils. We keep all the transmit and receive coil of same radius and number of turns. The tuning capacitor for all the coils remain the same. The following equations shows the self impedances of each coil. Since all the receive coils use the tuning capacitor in parallel, they get the same self impedance.

$$
\begin{aligned}
Z_{L1} &= \frac{Z_L}{1 + j\omega C} \\
Z_t &= R_t + j\omega L_t + \frac{1}{1 + j\omega C_t} \\
Z_r &= Z_{r1} = Z_{r2} = Z_{r3} \\
Z_r &= R + j\omega L
\end{aligned} \tag{6}
$$

To make the multi coil more robust , the coils are placed orthogonal to each other. Depending on the mutual coupling among the receive coils, we have divided the circuit analysis into two sub cases.The two arrangements can be seen in Figure 4 and Figure 5 whereas the mutual coupling has been computed using the equation 1.

3.1. Case 1. In the first arrangement the coils are orthogonal as well as same centered. The mutual coupling among the three coils, if centered along one point is zero. The equivalent circuit for such arrangement is shown in Figure 4. The reflected impedance equations are given by equation 7

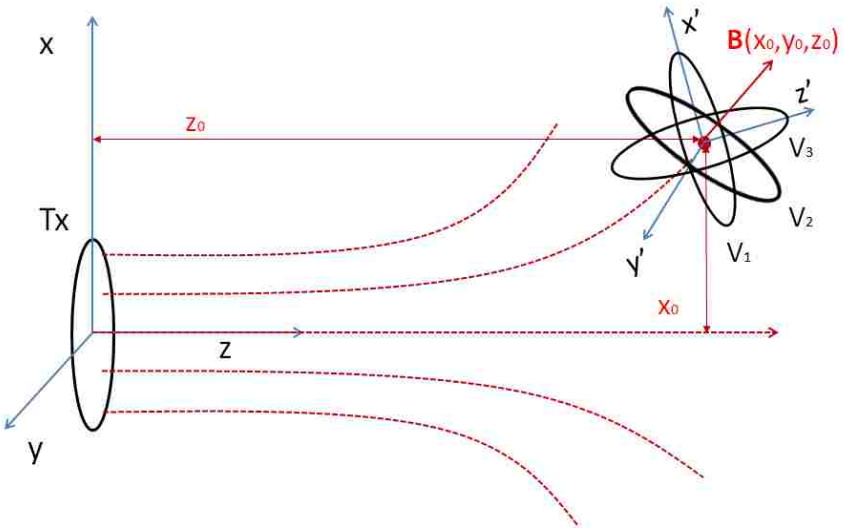

(a) Spherical configuration

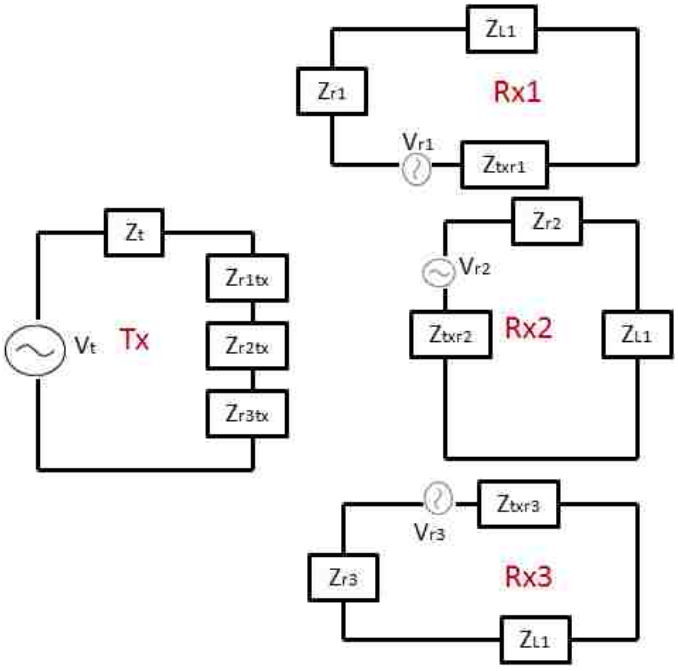

(b) Equivalent circuit model

Figure 4. Case 1: where$M_{r1r2} = M_{r2r3} = M_{r1r3} = 0$

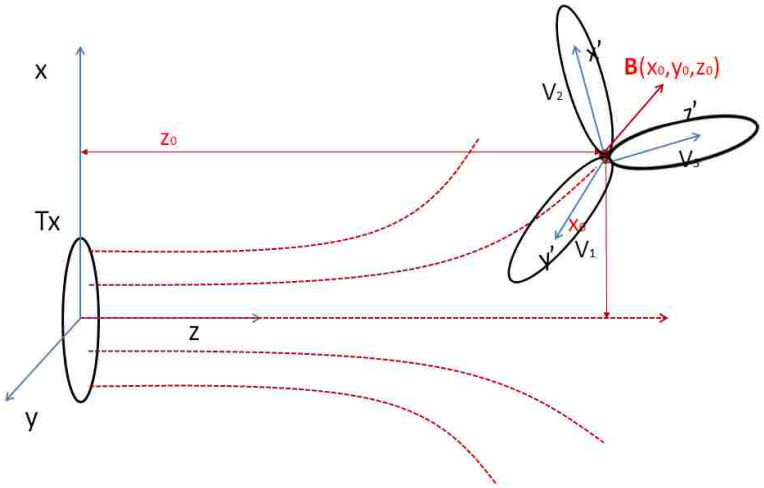

(a) Cubical configuration

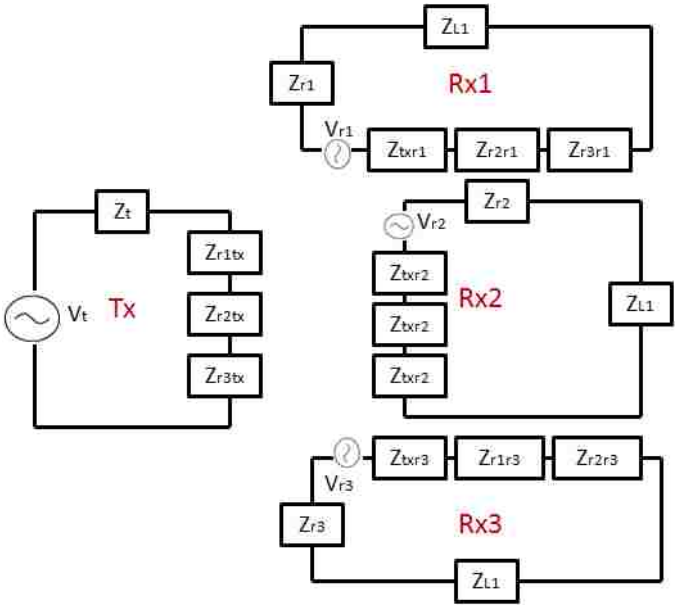

(b) Equivalent circuit model

Figure 5. Case 2: where $M_{r1r2} = M_{r2r3} = M_{r1r3} \neq 0$.

$$
\begin{aligned}
Z_{r1tx} &= \frac{\omega^2 M_{r1tx}^2}{Z_r + Z_{L1}}, \quad Z_{txr1} = \frac{\omega^2 M_{r1tx}^2}{Z_t} \\
Z_{r2tx} &= \frac{\omega^2 M_{r2tx}^2}{Z_r + Z_{L1}}, \quad Z_{txr2} = \frac{\omega^2 M_{r2tx}^2}{Z_t} \\
Z_{r3tx} &= \frac{\omega^2 M_{r3tx}^2}{Z_r + Z_{L1}}, \quad Z_{txr1} = \frac{\omega^2 M_{r3tx}^2}{Z_t}
\end{aligned}
$$

The induced voltage at each receiver coil is then given by equation 7. It can be observed that voltage induced in each receiver coil is independent of the other coils and given by

$$
V_{ri} = \frac{-j\omega M_{ritx} V_t}{Z_t}, \tag{7}
$$

3.2. Case 2. In the second arrangement the coils are orthogonal and placed at three corners of the cube. The mutual coupling among the three coils is no longer zero. The equivalent circuit for such arrangement is shown in Figure 5.

The reflected impedance equations are given by equation 8

$$
\begin{aligned}
Z_{r1tx} &= \frac{\omega^2 M_{r1tx}^2}{Z_r + Z_{L1}}, \quad Z_{txr1} = \frac{\omega^2 M_{r1tx}^2}{Z_t} \\
Z_{r2tx} &= \frac{\omega^2 M_{r2tx}^2}{Z_r + Z_{L1}}, \quad Z_{txr2} = \frac{\omega^2 M_{r2tx}^2}{Z_t} \\
Z_{r3tx} &= \frac{\omega^2 M_{r3tx}^2}{Z_r + Z_{L1}}, \quad Z_{txr1} = \frac{\omega^2 M_{r3tx}^2}{Z_t} \\
Z_{r1r2} &= \frac{\omega^2 M_{r1r2}^2}{Z_r + Z_{L1}}, \quad Z_{r1r3} = \frac{\omega^2 M_{r1r3}^2}{Z_r + Z_{L1}} \\
Z_{r2r1} &= \frac{\omega^2 M_{r2r1}^2}{Z_r + Z_{L1}}, \quad Z_{r2r3} = \frac{\omega^2 M_{r2r3}^2}{Z_r + Z_{L1}} \\
Z_{r3r1} &= \frac{\omega^2 M_{r3r1}^2}{Z_r + Z_{L1}}, \quad Z_{r3r2} = \frac{\omega^2 M_{r3r2}^2}{Z_r + Z_{L1}}
\end{aligned} \tag{8}
$$

The induced voltages at each receiver coil is then given by equation 9. It can be observed that voltage induced in each receiver coil has effect from the nearby coupling and voltage of the other coil detunes the coil from the operating frequency.

$$
\begin{aligned}
V_{r1} &= -j\omega \left[\frac{V_t M_{txr1}}{Z_t} + \frac{V_{r2} M_{r1r2}}{Z_r + Z_{L1}} + \frac{V_{r3} M_{r1r3}}{Z_r + Z_{L1}} \right] \\
V_{r2} &= -j\omega \left[\frac{V_t M_{txr2}}{Z_t} + \frac{V_{r1} M_{r1r2}}{Z_r + Z_{L1}} + \frac{V_{r3} M_{r2r3}}{Z_r + Z_{L1}} \right] \\
V_{r3} &= -j\omega \left[\frac{V_t M_{txr3}}{Z_t} + \frac{V_{r1} M_{r1r3}}{Z_r + Z_{L1}} + \frac{V_{r2} M_{r3r2}}{Z_r + Z_{L1}} \right]
\end{aligned}
\tag{9}
$$

The induced voltage equations can be represented in a matrix form of $AX = B$ as

$$
\begin{bmatrix}
1 & 0 & 0 & 0 \\
\frac{M_{txr1}}{Z_t} & 1 & \frac{M_{r1r2}}{Z_r+Z_{L1}} & \frac{M_{r1r3}}{Z_r+Z_{L1}} \\
\frac{M_{txr2}}{Z_t} & \frac{M_{r1r2}}{Z_r+Z_{L1}} & 1 & \frac{M_{r2r3}}{Z_r+Z_{L1}} \\
\frac{M_{txr3}}{Z_t} & \frac{M_{r1r3}}{Z_r+Z_{L1}} & \frac{M_{r3r2}}{Z_r+Z_{L1}} & 1
\end{bmatrix}
\begin{bmatrix} V_{tx} \\ V_{r1} \\ V_{r2} \\ V_{r3} \end{bmatrix}
=
\begin{bmatrix} 3 \\ 0 \\ 0 \\ 0 \end{bmatrix}
$$

4. SIMULATION RESULTS

We use Matlab to perform simulations. We consider case 1 configuration for our simulation. The reason for choosing case 1 configuration, is that mutual coupling among the three receive coil is zero and voltage induced at each coil is independent of the other two coils present nearby. Thus, all the three coils listens to the channel independently and the receiver then select the maximum voltage induced among the three coils.

Figure 6a illustrates different curves for different position of the rx coil with respect to tx coil. The tx coil is centered at (0,0,0) and is on the z-axis while the rx coil is centered at different locations to show the effect of mutual inductance at different directions in the

plane. It can be seen that the mutual inductance is maximum when both the rx and tx coils are on the same z-axis. The graph also shows placing the rx at (0,2,0), (0,2,2) and (2,2,2). Similarly, the mutual inductance is minimum when the rx coil is placed at (2,2,2).

Since keeping the rx coil on z-axis give the maximum mutual inductance, another illustration is shown in Figure 6b where the rx-coil is moved away from the tx coil along the z-axis. The curves are plotted with z = 2 m, 10 m, 15 m and 30 m. The plots clearly shows decay in the mutual inductance as the rx coil is moved away.

It can be observed from figure 6 that for a given distance the mutual inductance is maximum when the surface of the receive coil is either at zero degree or 90 degree. The reason is that all the three coils are orthogonal and at zero degree one of the coil (say coil one) is facing the transmit coil and couples strongly. When the multi coil receiver is rotated 90 degree coil two then faces the transmit coil and couples strongly. Similarly at 45 degree none of the coil is facing the transmit coil and we observe the minimum coupling at that angle. Figure 7 shows the decay of mutual coupling with increase in distance.

5. CONCLUSION

We have presented theoretical modeling and equivalent circuit analysis of multi coil channels in near field magneto inductive communication. The formulae for mutual coupling between two coils have been shown located at any point in the three dimensional space. The node equations in the circuit analysis were built by expanding the transformer equations. Multi coil with two different orthogonal arrangements was presented. It was shown that between the two arrangements: spherical configuration and cubical configuration, spherical configuration proves to induce more voltage and should be chosen to develop multi coil communication system.

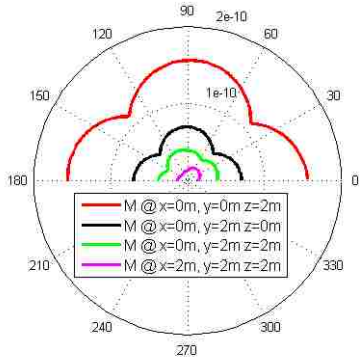

(a) When Rx coil is placed at different positions in space

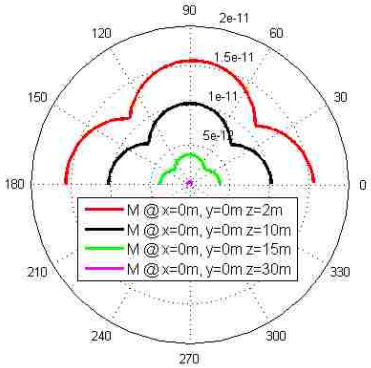

(b) When Rx is moved away from Tx on z-axis

Figure 6. Polar plot of mutual coupling between Tx and Rx coil

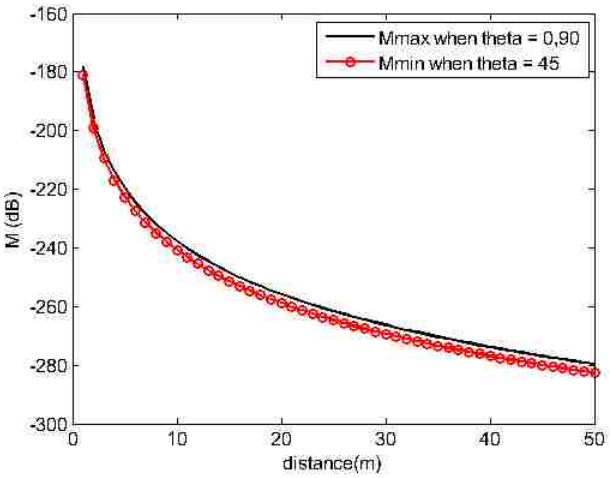

Figure 7. Mutual coupling with distance

REFERENCES

[28] *FreeLinc Near-Field Magnetic Induction Technology*. URL http://www.freelinc.com/downloads/FreeLinc/20NFMI/20White/20Paper.pdf.

[29] Johnson I Agbinya. Investigation of near field inductive communication system models, channels and experiments.(report). *Progress In Electromagnetics Research B*, 49: 129–153, April 2013. doi: doi:10.2528/PIERB12120512.

[30] N. Ahmed, J. Hoyt, A. Radchenko, D. Pommerenke, and Yahong Rosa Zheng. A multi-coil magneto-inductive transceiver for low-cost wireless sensor networks. In *Proc. Underwater Communications Networking Conf.*, pages 1–6, September 2014. URL http://ucomms.net/.

[31] S. Babic, F. Sirois, C. Akyel, and C. Girardi. Mutual inductance calculation between circular filaments arbitrarily positioned in space: Alternative to grover's formula. *IEEE Trans. Magn.*, 46(9):3591–3600, September 2010. ISSN 0018-9464. doi: 10.1109/TMAG.2010.2047651.

[32] S. Cheon, Y. H. Kim, S. Y. Kang, M. L. Lee, J. M. Lee, and T. Zyung. Circuit-model-based analysis of a wireless energy-transfer system via coupled magnetic resonances. *IEEE Transactions on Industrial Electronics*, 58(7):2906–2914, July 2011. ISSN 0278-0046. doi: 10.1109/TIE.2010.2072893.

[33] Marco Dionigi, Guido De Angelis, Antonio Moschitta, Mauro Mongiardo, and Paolo Carbone. A simple ranging system based on mutually coupled resonating circuits. *IEEE trans. Instrum. Measure*, 63(5), 2014.

[34] B. Gulbahar and O.B. Akan. A communication theoretical modeling and analysis of underwater magneto-inductive wireless channels. *IEEE Trans. Wireless Commun.*, 11 (9):3326–3334, September 2012. ISSN 1536-1276. doi: 10.1109/TWC.2012.070912.111943.

[35] M. Manteghi and A.A.Y. Ibraheem. On the study of the near-fields of electric and magnetic small antennas in lossy media. *IEEE Trans. Antennas Propag.*, 62(12): 6491–6495, Dec 2014. ISSN 0018-926X. doi: 10.1109/TAP.2014.2359499.

[36] S.A. Meybodi, M. Dohler, A.N. Askarpour, J. Bendtsen, and J.D. Nielsen. The feasibility of communication among pumps in a district heating system. *IEEE Antennas Propagat. Mag.*, 55(3):118–134, June 2013. ISSN 1045-9243. doi: 10.1109/MAP.2013.6586631.

[37] H. Nguyen, J.I. Agbinya, and J. Devlin. FPGA-based implementation of multiple modes in near field inductive communication using frequency splitting and MIMO configuration. *IEEE Trans. Circuits Syst. I, Reg. Papers*, 62(1):302–310, Jan 2015. ISSN 1549-8328. doi: 10.1109/TCSI.2014.2359716.

[38] A.P. Sample, D.A. Meyer, and J.R. Smith. Analysis, experimental results, and range adaptation of magnetically coupled resonators for wireless power transfer. *Industrial Electronics, IEEE Transactions on*, 58(2):544–554, Feb 2011. doi: 10.1109/TIE.2010.2046002.

[39] A. Sheinker, B. Ginzburg, N. Salomonski, L. Frumkis, and B.-Z. Kaplan. Localization in 3-D using beacons of low frequency magnetic field. *IEEE Trans. Instrum. Meas.*, 62(12):3194–3201, Dec 2013. ISSN 0018-9456. doi: 10.1109/TIM.2013.2270919.

[40] J.J. Sojdehei, P.N. Wrathall, and D.F. Dinn. Magneto-inductive (mi) communications. In *MTS/IEEE OCEANS Conf.*, volume 1, pages 513–519, November 2001. doi: 10.1109/OCEANS.2001.968775.

[41] Zhi Sun and I.F. Akyildiz. Magnetic induction communications for wireless underground sensor networks. *IEEE Trans. Antennas Propag.*, 58(7):2426–2435, July 2010. ISSN 0018-926X. doi: 10.1109/TAP.2010.2048858.

[42] H. Wegleiter, B. Schweighofer, C. Deinhammer, G. Holler, and P. Fulmek. Automatic antenna tuning unit to improve rfid system performance. *IEEE Trans. Instrum. Meas.*, 60(8):2797–2803, Aug 2011. ISSN 0018-9456. doi: 10.1109/TIM.2011.2122390.

III. EFFECTS OF METAL STRUCTURES ON MAGNETO-INDUCTIVE COUPLED COILS

Niaz Ahmed, Yahong Rosa Zheng, David Pommerenke

Dept. of Electrical & Computer Engineering

Missouri University of Science & Technology, Rolla, MO 65409

{namn3, zhengyr, davidjp}@mst.edu

ABSTRACT

This paper analyses the effects of metal structures in near-field Magneto-Inductive (MI) communication systems, where the transmitter and/or receiver coils may be close to large metal structures that has high magnetic permeability and conductivity. EMCoStudio simulations show that the presence of metal structure help to increase the coupling magnitude if placed nearby the transmit and receive coils, but reduces significant if placed between the transmit and receive coils.

1. INTRODUCTION

MI communications has attracted significant research interests in recent years. MI communication has been commonly used in nearfield touchless entry, RF identification (RFID) [50], underground sensing [53], and target localization [49, 47]. Sojdehei *et. al* [51] reported a underwater MI system that achieved 400 m communication range in sea water with low data rate. Sun and Akyildiz [52] describe magnetic induction for a underground wireless sensor networks. Meybodi *et. al* studied MI for district heating system with underground localization [48] [46]. Markham *et. al* studied underground 3D localization and tracking using MI systems. Agbinya [44] investigated MI for increasing near-field communication range.

One of the advantage MI exhibits over EM and acoustic is that MI performs similar in different medium such as air, water and underground. Unlike EM, MI mainly depends on the magnetic permeability and conductivity of the medium which allow MI to penetrate through solids, air and water similarly. This advantage of MI make MI the best choice to be used for applications which involve communication through different mediums. One of such application is a levee monitoring solution shown in Fig. 1 where MI sensor nodes can be use to monitor the health of I-wall.

Figure 1 shows a levee equipped with MI sensor nodes and base-station nodes. The sensor node monitors the I-wall which is often placed very close to the I-wall; while the base-station may be placed in either side of the I-wall in practical deployment. I-wall is constructed with iron bars which make the I-wall look like a metal plate that has high magnetic permeability and conductivity. Since the MI sensor nodes will be placed close by the I-wall, it is required to analyze the effect of metal plate on the magnitude of the coupling between the transmit and receive coils. This paper thus studies the effect of metal presence in the vicinity of coils. We simulate different cases to analyze the effect and the results show that when metal plate is placed between the transmit and receive coil the performance degrades whereas placing the coils on the side of the metal plate helps to couple more strongly.

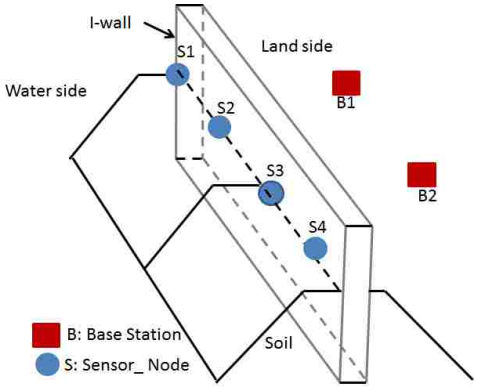

Figure 1. Levee health monitoring solution using MI communication.

2. MI COMMUNICATION MODEL

MI communication systems use well-tuned coils at the transmitter to create an alternating magnetic field which is a quasi-static field. The receive coils are coupled via the magnetic field in the near field region. The coupling can be measured by a coupling coefficient between the coils as the ratio of the flux that passes through the receive coil, relative to the total flux generated at the transmit coil.

The amount of mutual coupling that links the transmit and receive coils depends on the distance, orientation and presence of magnetic or conductive materials near the two coils. In general, the closer the transmitter and receiver coil, the greater is the mutual inductance. Similarly, if the two coils are perfectly aligned to each other in orientation, the mutual inductance will be maximum. Presence of magnetic material also greatly effects the communication depending on the magnetic permeability of the medium.

2.1. Magnetic Field Generated by Tx Coils. Assume the transmit coil is centered at the origin of a Cartesian coordinate system and is aligned with xy plane. The magnetic field created by the current loop at any point (x, y) in the xy plane is derived as [45]

$$\mathbf{B}(x,y) = \frac{\mu_0\mu_r Ik}{4\pi\sqrt{rx^3}}\left(K(k) + \frac{k^2(x+r)-2x}{2r(1-k^2)}E(k)\right)x\hat{\mathbf{x}} - \frac{\mu_0\mu_r Ik}{4\pi\sqrt{rx^3}}\left(K(k) - \frac{2-k^2}{2(1-k^2)}E(k)\right)y\hat{\mathbf{y}} \quad (1)$$

where μ_o is magnetic permeability constant, μ_r is the magnetic permeability of the medium, I is the current flowing through the coil, r is the radius of the coil and (x, y) denotes an arbitrary point from the origin.

To find the magnetic vector potential and then take the divergence of the magnetic vector potential, the derivation uses the first and second kind of elliptic integrals defined respectively, as

$$K(k) = \int_0^{\pi/2} \frac{d\alpha}{\sqrt{1-k^2\sin^2\alpha}} \quad (2)$$

and

$$E(k) = \int_0^{\pi/2} \sqrt{1 - k^2 \sin^2 \alpha} d\alpha \tag{3}$$

where k is defined as

$$k = \sqrt{\frac{4xr}{(x+r)^2 + y^2}}$$

Table 1 shows the magnetic permeability of different media. It can be seen that for vacuum, air and water, the value is close to 1, but for magnetic materials like iron, the magnetic permeability is as high as 80, which effects the strength of magnetic field around the material.

2.2. Induced Voltage at the Rx Coils. At the receiver side, voltage is generated as the induced emf with the change in magnetic flux (Φ). Magnetic flux can be expressed as the dot product of the magnetic field ($\mathbf{B}$) and the perpendicular area that the field passes through.

$$\Phi = \int \mathbf{B} \cdot d\mathbf{A} \tag{4}$$

Using Faraday's law of induction, the voltage induced at coil x can be written as:

$$V = \omega \frac{d\Phi}{dt} \tag{5}$$

Substituting eqn(4) in eqn(5) yields

$$V = \omega \mid B \mid A \cos(\beta) \tag{6}$$

where $\mathbf{B}$ is the transmitter magnetic field from the center of the Tx coil to the center of received coil, A is the area of the receiver coil and β is the angle formed between the magnetic field ($\mathbf{B}$) and normal to the receiver coil plane. $\mid B \mid$ is the constant magnitude of the magnetic field.

Table 1. Magnetic permeability of materials

Material	Magnetic Permeability
Vacuum	1.00000
Air	1.0000004
Water	0.999991
Iron	80

With configuration of three dimensional coils, each of the Rx coils independently couples with the magnetic field transmitted from the Tx coil and induces voltages V_1, V_2, V_3 respectively. The receiver node then selects the maximum of the three:

$$V_{recvd} = max(V_1, V_2, V_3) \tag{7}$$

3. PERFORMANCE EVALUATION

We consider a levee constructed with soil, rocks and metal plates. Since metals have higher magnetic permeability compared with that of air as shown in Table 1, we simulate the effect of metal plate on transmitting and receiving coils using EMCoStudio [43]. A three dimensional coil is created to represent the transmit and receiver sensor node and a metal plate to represent the I-wall, as shown in Fig. 2. Coils Rx1/Tx1, Rx2/Tx2 and Rx3/Tx3 are placed along y, z and x axis with radius 0.13 m, 0.1365 m and 0.143 m, respectively. Coils Tx3 & Rx3 are facing each other and coils Tx1 & Rx1 face the metal plate.

We simulate two major cases: when both Tx/Rx coils are placed on one side of the metal plate and when the Tx/Rx coils are placed across the metal plate. We used all the three coils to transmit independently and observed the effect of the transmit coil orientation with respect to metal plate. All the three coils set to transmit separately one at a time with

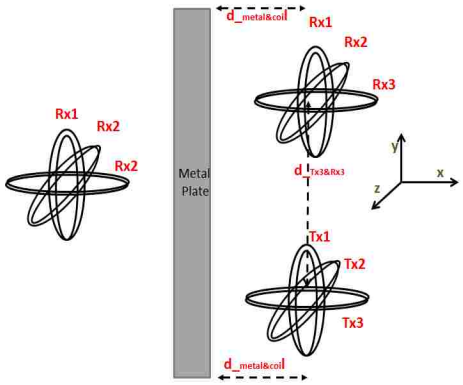

Figure 2. Simulation Setup: MI Sensor node modeled as three dimensional coils and placed on both sides of the I-wall

presence and absence of metal plate. The transmit coil was tested at different distance from the metal plate and the closest distance was 0.14 m which is a little more than the radius of the coil.

We use all the three coils to transmit independently and observe the effect of the transmit coil orientation with respect to metal plate. All the three coils set to transmit separately one at a time with presence and absence of metal plate. The transmit coil was tested at different distance with the metal plate and the closest distance was 0.14 m which is a little more than the radius of the coil.

3.1. Case 1: Coils Placed On The Same Side Of Metal Plate. When the transmit and receive coils are placed along the I-wall, the results are shown in Figure 3. In all the three sub-figures, one of the tx coil is set to transmit at a time and all the three coils of the rx coil induce the voltage. It can also be seen that when tx coil 3 is transmitting the rx coil 3 induces the maximum voltage due to facing each other. Figure 4 shows the simulation results of three three sub-cases. Figure 4a shows the scenario where we set both tx and rx coils to move away from the metal plate and see the effect on the received voltage. Figure 4b represents a scenario where we keep the rx coil close to the metal plate at distance $0.25m$ and move the tx coil $1m$ away from the metal plate. We simulate and record the induced

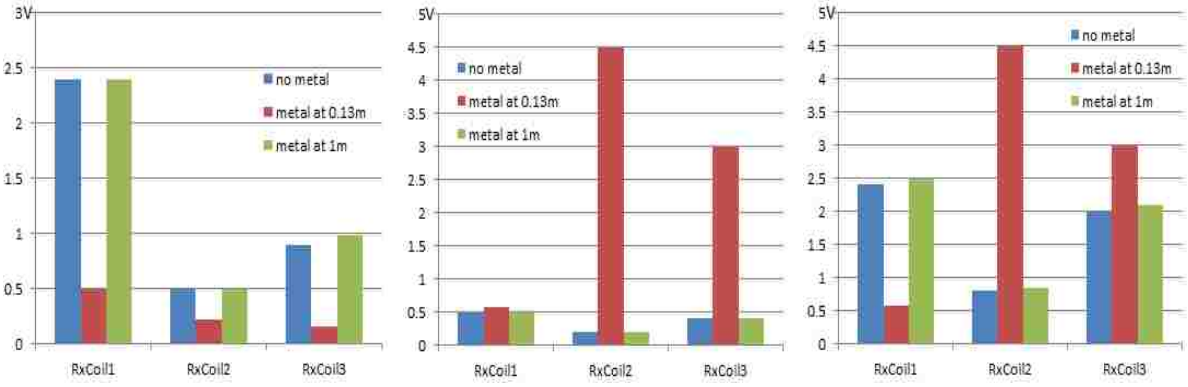

(a) When Tx coil 1 is set to transmit (b) When Tx coil 2 is set to transmit (c) When Tx coil 3 is set to transmit

Figure 3. One of the transmit coil is transmitting while all the receive coils are receiving. Results are without metal presence, with metal placed at 0.13m (edge of coils close to metal), and with metal placed at 1m from the edge off transmit coil 3. Tx and Rx coils are at the same distance away from the metal plate as shown in Figure 4

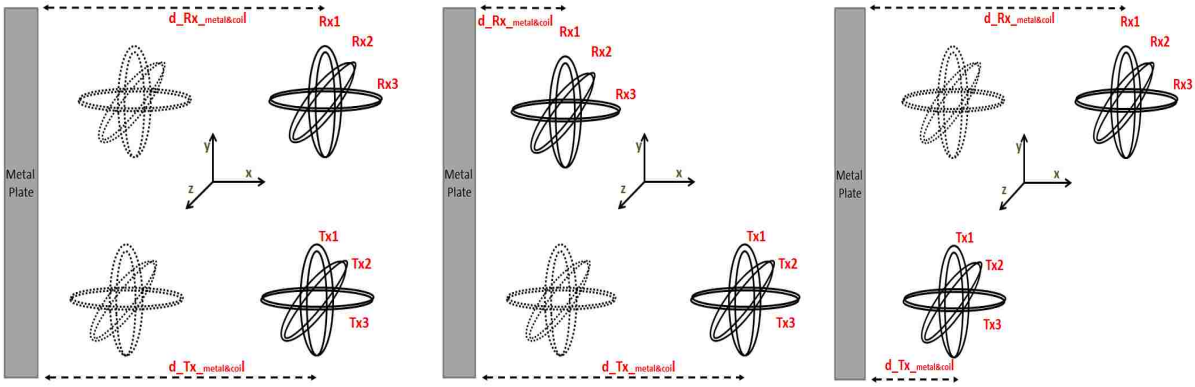

(a) Tx and Rx coils are on same distance from the metal plate (b) When Rx coil is close to the metal plate and Tx coil is moved away from the metal plate (c) When Rx coil is moved away from the metal plate and Tx coil is close to the metal plate

Figure 4. Case 1: When transmit and receive coils are placed on the same side of the metal plate

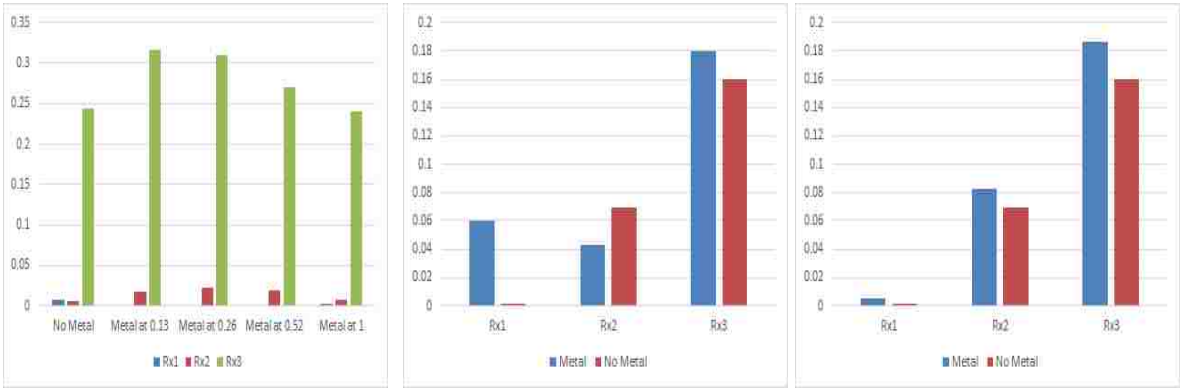

(a) Case 1a: Tx and Rx both are moved at the same distance away from the metal plate

(b) Case 1b: Rx is close to the metal plate and Tx is moved away from the plate

(c) Case 1c: Tx is close to the metal plate and Rx is moved away from the plate

Figure 5. Case 1 results: When transmit and receive coil are placed on the same side of the metal plate as shown in Figure 4. Metal plate enhances the received signal when metal is placed in the vicinity of the coils.

voltage in both presence and absence of metal plate. Similarly, Figure 4c represents a scenario where the tx coil is kept closer to the metal plate at distace $0.25m$ and move the rx coil at $1m$.

Figure 5 a,b,c shows results of Figure 4 a,b,c respectively. The results are shown for the tx3/rx3 coil only. It can be seen in Figure 6a that when metal plate is kept near the coils the induced voltage increases and as the coils are moved away from the metal plate, the induced voltage starts decreasing. It can also be noted that when the coils are moved $1m$ away from the metal plate the induced voltage becomes similar to when no metal was placed. This yields that at $1m$ distance the metal plate effects become negligible.

3.2. Case 2: Coils Placed On The Opposite Side Of Metal Plate. When the transmit and receive coils are on the opposite side of the I-wall, the simulation results are shown in 6 . It can be seen that there is a decrease in the received voltage when the metal plate is introduced between the two coils. The amount of decrease is not significant when Tx2 and Tx3 are set to transmit but is almost half when Tx1 is set to transmit.

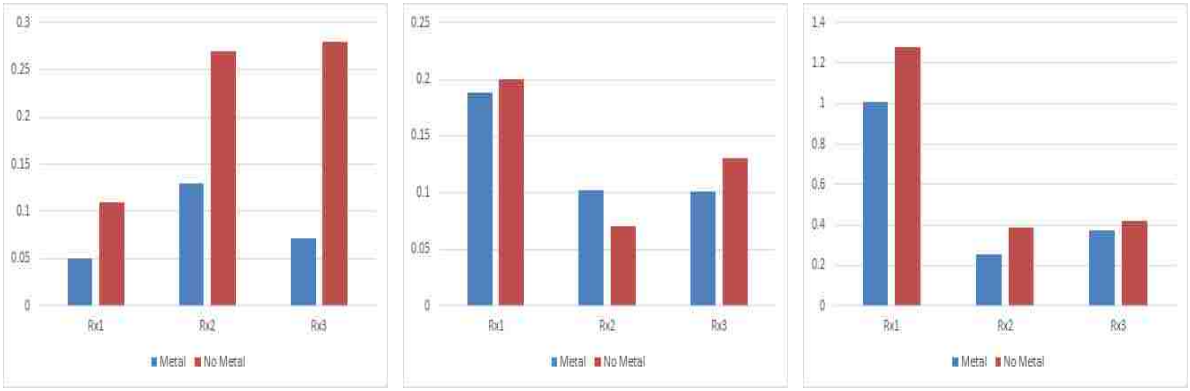

(a) When Tx coil 1 is set to transmit (b) When Tx coil 2 is set to transmit (c) When Tx coil 3 is set to transmit

Figure 6. Case 2 results: When transmit and receive coil are on the opposite side of the I-wall as shown in 2

.

The simulations thus shows that If the transmit coil is facing the metal plate, then it will have drastic effect and will result in poor communication. Other than facing the metal plate, the presence of metal coil leads to better communication when performed along the I-wall and almost similar communication when performed across the I-wall.

4. CONCLUSION

The paper present the mathematical model for MI communication and then evaluates the effect of metal presence on MI coils. Extensive simulation results are shown to help analyze the effect of metal and has been observed that metal present on one side of the coils enhance the induced voltage and reduces the induced voltage when the metal is placed in between the coils.

5. ACKNOWLEDGEMENT

This work is supported in part by the National Science Foundation grant #ECCS1408316 of the United States. We would also like to acknowledge Jeff Birt for his help with drawing some of the figures.

REFERENCES

[43] URL https://www.emcos.com/?products=emc-studio.

[44] Johnson I Agbinya. Investigation of near field inductive communication system models, channels and experiments.(report). *Progress In Electromagnetics Research B*, 49: 129(25), 2013-04-01.

[45] Kevin Kuns. Calculation of magnetic field inside plasma chamber. *IEEE Commun. Mag.*, August 2007.

[46] Andrew Markham, N. Trigoni, D.W. Macdonald, and S.A. Ellwood. Underground localization in 3-d using magneto-inductive tracking. *Sensors Journal, IEEE*, 12(6): 1809–1816, June 2012. ISSN 1530-437X. doi: 10.1109/JSEN.2011.2178064.

[47] Andrew Markham, N. Trigoni, D.W. Macdonald, and S.A. Ellwood. Underground localization in 3-d using magneto-inductive tracking. *IEEE Sensors J.*, 12(6):1809–1816, June 2012. ISSN 1530-437X. doi: 10.1109/JSEN.2011.2178064.

[48] S.A. Meybodi, J. Nielsen, J. Bendtsen, and M. Dohler. Magneto-inductive underground communications in a district heating system. In *Communications (ICC), 2011 IEEE International Conference on*, pages 1–5, June 2011. doi: 10.1109/icc.2011.5963067.

[49] S.A. Meybodi, J. Nielsen, J. Bendtsen, and M. Dohler. Magneto-inductive underground communications in a district heating system. In *IEEE ICC 2011*, pages 1–5, June 2011. doi: 10.1109/icc.2011.5963067.

[50] C.M. Roberts. Radio frequency identification (rfid). *Computers and security*, 25(1): 18 – 26, 2006. ISSN 0167-4048. doi: http://dx.doi.org/10.1016/j.cose.2005.12.003.

[51] J.J. Sojdehei, P.N. Wrathall, and D.F. Dinn. Magneto-inductive (mi) communications. In *OCEANS, 2001. MTS/IEEE Conference and Exhibition*, volume 1, pages 513–519 vol.1, 2001. doi: 10.1109/OCEANS.2001.968775.

[52] Zhi Sun and I.F. Akyildiz. Magnetic induction communications for wireless underground sensor networks. *Antennas and Propagation, IEEE Transactions on*, 58(7): 2426–2435, July 2010. ISSN 0018-926X. doi: 10.1109/TAP.2010.2048858.

[53] Zhi Sun and I.F. Akyildiz. Magnetic induction communications for wireless underground sensor networks. *IEEE Trans. Antennas Propag.*, 58(7):2426–2435, July 2010. ISSN 0018-926X. doi: 10.1109/TAP.2010.2048858.

IV. MULTI-COIL MI BASED MAC PROTOCOL FOR WIRELESS SENSOR NETWORKS

Niaz Ahmed, Yahong Rosa Zheng, David Pommerenke

Dept. of Electrical & Computer Engineering

Missouri University of Science & Technology, Rolla, MO 65409

{namn3, zhengyr, davidjp}@mst.edu

ABSTRACT

Medium Access Control (MAC) protocol is an important metric of wireless sensor networks because of its high impact on network performance. This paper proposes an energy efficient MAC protocol that can be used for both terrestrial and underwater wireless sensor networks. The state transition diagram has been presented in the paper and current consumption for each state has been recorded to evaluate the energy efficiency of the proposed MAC protocol.

1. INTRODUCTION

Medium Access Control (MAC) protocol is an important quality metric of terrestrial and underwater wireless sensor networks. An inefficient MAC layer can result in heavy packet collisions, delayed communication and significant energy wastage. Wireless sensor networks offer a number of challenges for real time MAC layer protocol implementation and the major challenge is energy consumption [75] because most of the wireless sensor networks applications require deployment of sensor nodes with limited energy resources . The challenge becomes more severe with slow speed of propagation, low data rates and high processing power requirement in case of underwater acoustic sensor networks [69].

During recent years researchers have proposed a number of energy efficient MAC protocols for both terrestrial [78, 77, 56, 60, 61, 64, 62, 63, 66, 67, 71, 73, 74] and underwater wireless sensor networks [76, 57, 58, 59, 65, 68, 54, 70, 72] but unfortunately, only a few techniques have been prototyped as testbeds. We believe that real time implementation of the MAC layer for wireless sensor networks is a real need and propose a contention based MAC protocol with magneto-inductive(MI) based communication.

In this paper we present the proposed energy efficient MAC layer protocol for wireless sensor networks. The sensor node is capable of magneto inductive communication which allows the sensor node to be deployed for both terrestrial and underwater sensor networks [55]. This paper present the design decisions, state transition diagram and implementation details of the proposed MAC layer.

2. OUR DESIGN RATIONALE

The primary goal is to design an energy efficient MAC protocol for a sensor node in wireless sensor networks. Our goal stems from the fact that monitoring applications require the sensor node to run for long time without replacing the battery power. We chose to use MI communication that allow the sensor node to work both in terrestrial and underwater wireless sensor networks.

Table 1 shows the common sources of energy consumption for a MAC protocol. All these sources contribute in energy losses in an idle mode when the sensor is listening to the channel. To keep the sensor node to consume the minimum possible energy in these cases we:

- Isolate the power of each component in the sensor node design. This allows the sensor node to shut down the components that are inactive. The software controls the power to each component and decides if the component needs to be ON/OFF. This significantly reduce the overall power consumption of the system.

Table 1. Common Sources of Energy Consumption

Idle Listening	When the sensor node is listening to the channel in order to receive an upcoming packet
Packet Collision	When two or more nodes start to communicate simultaneously and result in collision of the simultaneously transmitted packets.
Packet Overhearing	When a sensor node receives and tries to decode a packet that is not destined for it.
Control Packet Overhead	When a sensor node include additional control information to the actual payload.

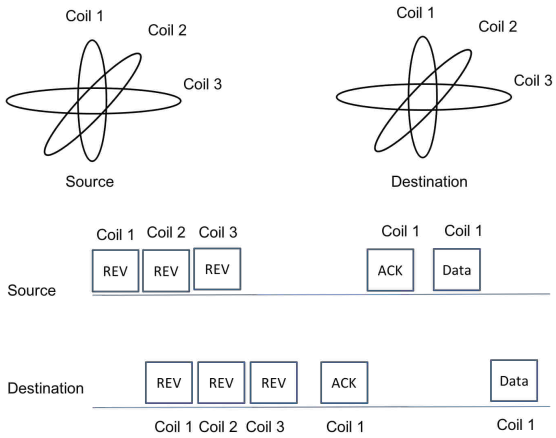

Figure 1. Packet exchange information between source and destination when initiating a communication

- Sense the channel for the carrier before transmitting a packet and at the same time exploit the directional nature of MI communication to avoid collision.
- Keep three separate packet types of different length to lesser the overhead bytes.

3. PROPOSED MAC ALGORITHM

Figure 1 shows packet exchange information between two nodes: source and destination. The source initiates the communication by sending a reservation packet (REV) to the other node. As MI coils are directional and depend heavily on transmit & receive coil's

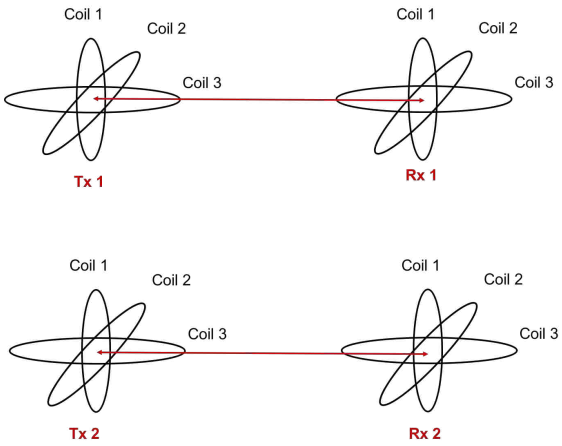

Figure 2. Two nodes can simultaneously transmit data packets to other nodes if the strongest coil pair is different.

orientation, the sensor node uses three dimensional coil for reliable and omni-directional communication. It is to be noted that the sensor node uses all the three coils to listen to the channel but use only one of the three coil to transmit at a given time. Thus the same REV packet is being sent three time from each of the three coils of the sensor node.

After the packet reaches the destination, the receiver sensor node compares the received packet sent by the three coils and records the coil pair that receives the strongest signal. The acknowledgment packet (ACK) is then sent back by using the coil with strongest RSSI. The two nodes then use the selected transmit & receive coil pair for further communication.

The directional nature of the MI coils and using the strongest transmit receive coil also allow nearby nodes to communicate with each other. Figure 2 shows a simple case where Tx1 & Rx1 communicates with coil 1 being the strongest coil and Tx2 & Rx2 also communicates with coil 2 being the strongest coil.

3.1. State Transition Diagram. The sensor node is programmed to remain in one of the five states: Idle, Receive, Channel Sensing, Data Acquire and Transmit states and the state transition diagram is shown in Figure 3.

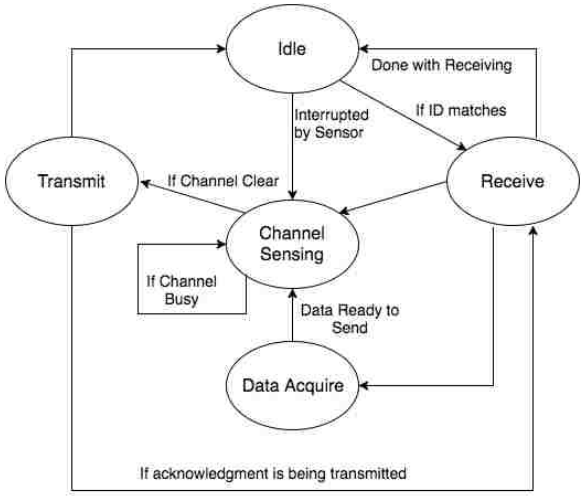

Figure 3. State transition diagram of the proposed MAC protocol

The sensor node starts with initialization and enters the Idle state which is an extreme low power state. The receiver IC is the only component that is running and is listening to the channel. The sensor node remains in the idle state until there is an interrupt from the sensor or a packet is received with correct ID. If an interrupt has been occurred, the sensor node prepares the transmit packet and enters the channel sensing mode. In case of the packet being received with the correct ID the sensor node enters to the receiving state.

Once the sensor node receives a packet and the ID matches the sensor node's ID, the sensor node enters the Receiving state. During this state the sensor node decodes the packet. If the received packet is a hand shaking packet, the sensor node prepares the packet to send back the acknowledgment and goes to Channel Sensing state. If the received packet is the data packet, the sensor node remains in the Receive state until the last byte of data is received. After receiving the last data packet, the sensor node goes to idle state. If the received packet requires the sensor node to transmit the sensor data, the sensor node then goes to the Data Acquire state.

In the Data Acquire state, the sensor node turns ON the sensors and collects the data from the interfaced sensors. The acquired data is formed into a packet and sensor node goes to Channel Sensing state.

The Channel Sensing state is the important state and key part of the proposed MAC protocol. Whenever a packet is being ready to be transmitted, the sensor node enters the Channel Sensing state. During this state the sensor node senses the channel to see if the channel is busy or available. The sensor node remains in the Channel Sensing state if the sensor node detects a nearby carrier and will go to Transmit state only when the channel is available.

During the Transmit state, the sensor node turns ON the transmitter circuitry and sends out the packet. If the transmitted packet is hand shaking packet, the sensor node goes to the Receive state as the sensor node expects an acknowledgment. Other than hand shaking packet, the sensor nodes enters the Idle state after the packet is being transmitted.

3.2. Packet Types Used. Figure 4 shows the three different types of packets used in the proposed MAC layer: Reservation packet (REV), Acknowledgment (ACK) and Data Packet. All the three packets start with one byte carrier letting the receiver sensor node to set up and ends with one byte EOF which indicates the end of the packet.

REV packet is used to initiate the communication between the two nodes. This is the hand shaking packet where the source sends a 13 byte packet. The carrier byte is followed by a one byte preamble allowing the receiver sensor node to start decoding the target ID. The preamble is then followed by a four byte target ID which the sensor node compares with the programmed ID and will forward the rest of packet only if the ID matches. If the ID does not match the packet is dropped by the sensor node. The next byte is the packet Id which identify whether the packet is REV, ACK or Data. Since the REV packet is the first packet of the transmission the sensor node includes the one byte transmit coil information. The purpose of the transmit coil information is to let the receiver sensor node know which coil is best suited for the two nodes to communicate.

After successful reception of the REV packet, the receiver sensor node reply with an ACK. The ACK is a five byte packet starting with one byte carrier and then followed by the one byte packet ID. The ACK also includes the transmit and receive coil information that can be then used for further communication.

Once the ACK is received the two sensor nodes are ready to exchange data packets. The data packet contains the sensor data or other information need to be transmitted which can vary between 1 to 16 bytes.

Carrier	Preamble	Target ID	Packet ID	Tx ID	Tx Coil ID	EOF
1 byte	1 byte	4 bytes	1 byte	4 bytes	1 byte	1 byte

Reservation Packet

Carrier	Packet ID	Tx Coil ID	Rx Coil ID	EOF
1 byte	1 byte	1 byte	1 byte	1 byte

Acknowledgment

Carrier	Packet ID	Data Packets	EOF
1 byte	1 byte	1 byte – 16 bytes	1 byte

Data Packet

Figure 4. The three packet types being used in the proposed MAC protocol

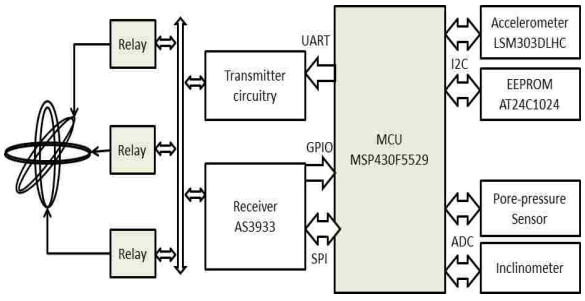

Figure 5. Block Diagram of the low-power sensor node with MI communication and sensing capabilities

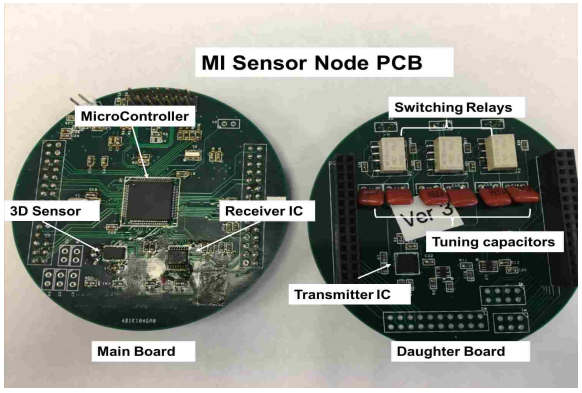

Figure 6. Printed Circuit Board (PCB) of sensor node. Antenna coils are not shown.

4. IMPLEMENTATION DETAILS

The block diagram of MI sensor node is shown in Figure 5 and the PCB hardware is shown in Figure 6, where micro-controller is the main controlling unit. The common micro-controller families that are being used in sensor network applications are Microchip PIC family, TI MSP430 family and Atmega family. PIC micro-controllers offer ultra low power consumption whereas Atmega offers high performance. We chose MSP430 family which is better suited for applications with high performance and lower power consumption. The micro-controller we are using in our sensor design is MSP430F5529 which is 16 bit ultra low power micro-controller with 128 KB Flash and 8 KB RAM.

The micro-controller uses the serial and ADC peripheral to interface with the other components. I2C bus is used to interface with accelerometer and memory chip. The analog sensors: pore pressure and inclinometer use the 12-bit ADC peripheral to connect with micro-controller. The micro-controller forwards the data to the transmitter IC (ATA5276) through Universal Asynchronous Receive and Transmit (UART) port. The micro-controller communicates with the receiver IC (AS3933) through GPIO pins and SPI serial interface. The control configurations are exchanged through SPI bus and received data is transferred from the receiver IC to micro-controller using GPIO pins.

Table 2. Current Consumption in Each State

Idle	Receive	Data Acquire	Channel Sensing	Transmit
50 uA	200 uA	250 uA	200 uA	1.12 mA

Three coils in spherical configuration, along with their matched tuning capacitors, are connected to the transmitter or receiver via a multiplexer. All three coils independently receive the three signals, which are fed to the three input ports of the AS3933 simultaneously; which then forwards the signal with highest strength to the micro-controller.

Table 2 shows the current requirement of the sensor node in each of the state. The sensor node is battery powered and require power supply of 3.6 V. It can be seen that in Idle state the current consumption is ultra low which keeps the overall energy consumption of the sensor node extremely low.

Table 3 shows the components that are ON or OFF during a specific state. During Idle state the power consumption is minimum as receiver IC is the only component that is kept ON. The MCU is in deep sleep mode and the other components are kept OFF. During the Receive state, the receiver IC wakes up the micro-controller which then receives the data. During the Data Acquire state, the micro-controller turns ON the sensor power, acquires the data and then turns OFF the sensor power. During the Channel Sensing state the two active components are micro-controller and the receiver IC. The receiver IC sense the channel and the micro-controller keep track of the sensing time. During the Transmit state, the micro-controller turns OFF all other components and turns ON the transmitter power.

Table 3. Active and In-Active components in each state

Working Mode	Components	Power Mode
Idle State	Micro-Controller	Sleep
	Receive Circuitry	ON
	Transmit Circuitry	OFF
	Sensors	OFF
Receive State	Micro-Controller	ON
	Receive Circuitry	ON
	Transmit Circuitry	OFF
	Sensors	OFF
Date Acquire State	Micro-Controller	ON
	Receive Circuitry	OFF
	Transmit Circuitry	OFF
	Sensors	ON
Channel Sensing State	Micro-Controller	ON
	Receive Circuitry	ON
	Transmit Circuitry	OFF
	Sensors	OFF
Transmit State	Micro-Controller	ON
	Receive Circuitry	OFF
	Transmit Circuitry	ON
	Sensors	OFF

5. CONCLUSION

The paper presents an energy efficient MAC layer protocol for wireless sensor networks. The MI based sensor design has been presented and believed to bring an insight in the terrestrial and underwater research community. State diagram of the MAC protocol is described and power consumption in each state is given to get the idea of the power in each state.

REFERENCES

[54] C-MAC: A TDMA-Based MAC Protocol for Underwater Acoustic Sensor Networks. *2009 International Conference on Networks Security, Wireless Communications and Trusted Computing*, 1:728–731, 2009.

[55] N. Ahmed, J. Hoyt, A. Radchenko, D. Pommerenke, and Y. R. Zheng. A multi-coil magneto-inductive transceiver for low-cost wireless sensor networks. In *Underwater Communications and Networking (UComms), 2014*, pages 1–5, Sept 2014. doi: 10.1109/UComms.2014.7017135.

[56] B.a. Alsaify and D.R. Thompson. Pendulum: An energy efficient protocol for Wireless Sensor Networks. *Sensors Applications Symposium (SAS), 2010 IEEE*, pages 7–11, 2010. doi: 10.1109/SAS.2010.5439409.

[57] Zahra Azar and M.T. Manzuri. A latency-tolerant MAC protocol for underwater acoustic sensor networks. *Control Automation and Systems (ICCAS), 2010 International Conference on*, pages 849–854, 2010. URL `http://ieeexplore.ieee.org/xpls/abs{\_}all.jsp?arnumber=5669755`.

[58] Keyu Chen, Maode Ma, En Cheng, Fei Yuan, and Wei Su. A Survey on MAC Protocols for Underwater Wireless Sensor Networks. *IEEE Communications Surveys & Tutorials*, 16(3):1433–1447, 2014. ISSN 1553-877X. doi: 10.1109/SURV.2014.013014.00032. URL `http://ieeexplore.ieee.org/lpdocs/epic03/wrapper.htm?arnumber=6757189`.

[59] Jinyong Cheon and Ho-shin Cho. A delay-tolerant OFDMA-based MAC Protocol for Underwater Acoustic Sensor Networks. pages 1–4, 2011.

[60] Sung Chan Choi, Jang Won Lee, Yeonsoo Kim, and Hakjin Chong. An energy-efficient MAC protocol with random listen-sleep schedule for wireless sensor networks. *IEEE Region 10 Annual International Conference, Proceedings/TENCON*, 2007. ISSN 0886-1420. doi: 10.1109/TENCON.2007.4428925.

[61] Xenofon Fafoutis. Medium Access Control in Energy Harvesting - Wireless Sensor Networks Xenofon Fafoutis. 2014.

[62] Y Gadallah and M Jaafari. A Reliable Energy-Efficient 802.15.4-Based MAC Protocol for Wireless Sensor Networks. *Wireless Communications and Networking Conference (WCNC), 2010 IEEE*, pages 1–6, 2010. doi: 10.1109/wcnc.2010.5506284.

[63] Xiao Han, Lei Shu, Yuanfang Chen, and Hairui Zhou. WX-MAC: An Energy Efficient MAC Protocol for Wireless Sensor Networks. *2013 IEEE 10th International Conference on Mobile Ad-Hoc and Sensor Systems*, pages 423–424, 2013. doi: 10.1109/MASS.2013.15. URL `http://ieeexplore.ieee.org/lpdocs/epic03/wrapper.htm?arnumber=6680274`.

[64] Yejun He and Xiao Wang. An Aloha-Based Improved Anti-Collision Algorithm for RFID Systems. (August):86–95, 2013.

[65] Chin Cheng Hsu, Kuang Fu Lai, Cheng Fu Chou, and Kate Ching Ju Lin. ST-MAC: Spatial-temporal MAC scheduling for underwater sensor networks. *Proceedings - IEEE INFOCOM*, pages 1827–1835, 2009. ISSN 0743166X. doi: 10.1109/INFCOM.2009.5062103.

[66] Youngmin Kim, Hyojeong Shin, and Hojung Cha. Y-MAC: An energy-efficient multi-channel MAC protocol for dense wireless sensor networks. *Proceedings - 2008 International Conference on Information Processing in Sensor Networks, IPSN 2008*, pages 53–63, 2008. doi: 10.1109/IPSN.2008.27.

[67] Dongho Lee and Kwangsue Chung. RA-MAC: An energy efficient and low latency MAC protocol using RTS aggregation for wireless sensor networks. *2008 International Conference on Advanced Technologies for Communications*, pages 150–153, 2008. doi: 10.1109/ATC.2008.4760542. URL http://ieeexplore.ieee.org/xpl/articleDetails.jsp?arnumber=4760542.

[68] Wen Hwa Liao and Chih Chien Huang. SF-MAC: A spatially fair MAC protocol for underwater acoustic sensor networks. *IEEE Sensors Journal*, 12(6):1686–1694, 2012. ISSN 1530437X. doi: 10.1109/JSEN.2011.2177083. URL http://ieeexplore.ieee.org/xpls/abs{_}all.jsp?arnumber=6086556.

[69] Deven Makhija, P Kumaraswamy, and Rajarshi Roy. Challenges and Design of Mac Protocol for Underwater Acoustic Sensor Networks. *Electrical Communication*, pages 0–5, 2006.

[70] Min Kyoung Park and Volkan Rodoplu. UWAN-MAC: An energy-efficient MAC protocol for underwater acoustic wireless sensor networks. *IEEE Journal of Oceanic Engineering*, 32(3):710–720, 2007. ISSN 03649059. doi: 10.1109/JOE.2007.899277.

[71] National Radio and Science Conference. C21 . E2MAC : An Energy-Efficient MAC Protocol for Wireless Sensor Networks. pages 244–251, 2014.

[72] Sumi A. Samad, S. K. Shenoy, G. Santhosh Kumar, and P. R Saseendran Pillai. RMAC-M: Extending the R-MAC protocol for an energy efficient, delay tolerant underwater acoustic sensor network application with a mobile data mule node. *Proceedings of the 2011 International Symposium on Ocean Electronics, SYMPOL-2011*, pages 217–223, 2011. doi: 10.1109/SYMPOL.2011.6170523.

[73] Shama Siddiqui and Sayeed Ghani. ES-MAC: Energy Efficient Sensor-MAC protocol for Wireless Sensor networks. *2013 10th IEEE INTERNATIONAL CONFERENCE ON NETWORKING, SENSING AND CONTROL (ICNSC)*, pages 28–33, 2013. ISSN 1810-7869. doi: 10.1109/ICNSC.2013.6548706. URL http://ieeexplore.ieee.org/lpdocs/epic03/wrapper.htm?arnumber=6548706.

[74] Lei Tang, Yanjun Sun, Omer Gurewitz, and David B. Johnson. PW-MAC: An energy-efficient predictive-wakeup MAC protocol for wireless sensor networks. *Proceedings - IEEE INFOCOM*, pages 1305–1313, 2011. ISSN 0743166X. doi: 10.1109/INFCOM.2011.5934913.

[75] A. Willig. Wireless sensor networks: Concept, challenges and approaches. *Elektrotechnik und Informationstechnik*, 123(6):224–231, 2006. ISSN 0932383X. doi: 10.1007/s00502-006-0351-1.

[76] Peng Xie and Jun-Hong Cui. R-MAC: An Energy-Efficient MAC Protocol for Underwater Sensor Networks. *International Conference on Wireless Algorithms, Systems and Applications (WASA 2007)*, (0644190):187–198, 2007. doi: 10.1109/WASA.2007.37. URL http://ieeexplore.ieee.org/lpdocs/epic03/wrapper.htm?arnumber=4288230.

[77] W. Ye, J. Heidemann, and D. Estrin. An energy-efficient MAC protocol for wireless sensor networks. *21st Conference of the IEEE Computer and Communications Societies*, 3:1567–1576, 2002. ISSN 0743-166X. doi: 10.1109/INFCOM.2002.1019408. URL http://ieeexplore.ieee.org/lpdocs/epic03/wrapper.htm?arnumber=1019408.

[78] Ming Zhang and Suoping Wang. An novel energy-efficient MAC protocol based on collision avoidance for wireless sensor networks. *Wireless Communications, Networking and Mobile Computing, 2009. WiCom'09. 5th International Conference*, (08):1–4, 2009. URL http://ieeexplore.ieee.org/xpls/abs{_}all.jsp?arnumber=5303266.

SECTION

2. SUMMARY AND CONCLUSIONS

A low-cost and low power three coil MI communication system has been designed and implemented for wireless sensor network applications. Different transmit and receive configurations have been investigated to choose the optimal low power configuration for the transceiver. The hardware and software implementation have been explained in detail and field tests have been performed to demonstrate the promising communication range and robust performance of the sensor node. Theoretical modeling and equivalent circuit analysis of multi coil channels in near field magneto inductive communication have been provided. Simulations have also been performed in EMC Studio to observe the effect of the presence of metal on MI communication. At the end an energy efficient MAC layer protocol for Magneto Inductive wireless sensor networks has been proposed and implemented to offer a complete solution for wireless sensor network applications.

VITA

Niaz Ahmed is born in Pakistan in 1988. He has received the B.S. degree in telecommunication engineering from NUCES-FAST university and M.S. degree in computer engineering from CASE University, Islamabad, Pakistan, in 2010 and 2012, respectively. He began his Ph.D study in August 2013 at the Department of Electrical and Computer Engineering at Missouri University of Science and Technology (formerly: University of Missouri-Rolla), USA. His research interests include underwater wirless sensor networks using Magneto Inductive communication. He received his Ph.D. degree in Electrical Engineering from Missouri University of Science and Technology in May 2017.